Studies on Semiconducting Polymer-Electrolyte and Conducting Polymer-Retinal Tissue Interfaces

A Thesis

submitted in partial fulfillment for the degree of

MASTER OF SCIENCE

as a part of the Integrated Ph.D programme

(Materials Science)

by

VINI GAUTAM

CHEMISTRY AND PHYSICS OF MATERIALS UNIT
JAWAHARLAL NEHRU CENTRE FOR ADVANCED SCIENTIFIC RESEARCH
(A Deemed University)
Bangalore – 560 064

AUGUST 2010

To my Parents

DECLARATION

I hereby declare that the matter embodied in the thesis entitled "**Studies on Semiconducting Polymer-Electrolyte and Conducting Polymer-Retinal Tissue Interfaces**" is the result of investigations carried out by me at the Chemistry and Physics of Materials Unit, Jawaharlal Nehru Centre for Advanced Scientific Research, Bangalore, India under the supervision of Prof. K. S. Narayan and that it has not been submitted elsewhere for the award of any degree or diploma.

In keeping with the general practice in reporting scientific observations, due acknowledgment has been made whenever the work described is based on the findings of other investigators.

Vini Gautam

CERTIFICATE

I hereby certify that the matter embodied in this thesis entitled "**Studies on Semiconducting Polymer-Electrolyte and Conducting Polymer-Retinal Tissue Interfaces**" has been carried out by Ms. Vini Gautam at the Chemistry and Physics of Materials Unit, Jawaharlal Nehru Centre for Advanced Scientific Research, Bangalore, India under my supervision and that it has not been submitted elsewhere for the award of any degree or diploma.

Prof. K. S. Narayan
(Research Supervisor)

Acknowledgments

I am grateful to my research advisor Prof. K.S.Narayan for his guidance throughout this work. He always gave me the opportunity to explore and venture into whatever new I wanted to learn.

I thank Prof. C.N.R. Rao for being a source of inspiration. I am also thankful to all other faculties of JNCASR for offering various courses related to Chemistry and Physics of materials. The courses built up my enthusiasm for research in this field. I also thank Prof. S.K.Sikdar for teaching the neuroscience course in IISc and for the useful discussions about my research work.

I thank Dr. Ajoy Vincent (Narayana Nethrayalaya) for his useful suggestions and comments and Dr. N.K. Dhingra (NBRC) for letting me visit his lab and learning the retina isolation procedure. I also thank Dr. Prakash (Animal Facility, JNCASR) for his help and cooperation.

Special thanks to my present lab mates Manu, Monojit, Sachi, Anshuman, Arun, Satya, Ravi, Vijay and Balaraju for a wonderful work environment. They all have been very helpful and very friendly. I have learnt a lot from them as well as my past lab mates Arun and shruti.

I would also like to acknowledge all my Int. PhD. 2007 batch mates Piyush, Soumik, Bivas, Nitesh, Abhay, Nisha, Ritu and Urmi. I enjoyed spending time with them throughout these three years.

I also thank all my friends in CPMU, MBGU, EOBU, EMU and TSU whom I have had various scientific discussions with and also enjoyed many extracurricular

activities in the Hostel. Their company has made my stay in JNCASR very homely.

Last but not the least, its my family's constant encouragement that drives me every moment. I would like to thank my grandparents, my mom, dad and my brother for all their love and support.

Outline

Two research problems have been addressed in this thesis. Both the problems involve the use of Conjugated Polymers. The first problem undertaken revolves around the photoexcitation of a semiconducting polymer-liquid electrolyte system. The system has been probed using photo-voltage and photo-capacitance measurements.

The second problem involves extracellular recordings of the light-evoked electrical activity from a mammalian retina. The aim is to study the changes induced in these signals when the properties of the recording electrodes are changed, precisely, when the recording electrodes are modified with a conducting polymer. The methods of study also include some basic noise analysis.

Chapter 1 is a general introduction to the properties of conjugated polymers. It also includes a brief summary of the features of a semiconductor-electrolyte interface.

Chapter 2 includes the experimental methods, results and analysis of the work done on semiconducting polymer-electrolyte devices.

Chapter 3 is an introduction to the electrical signal processes in the retina and some basic concepts of the extracellular recording techniques.

Chapter 4 summarizes the experiments and analysis of results obtained from the extracellular recordings of a retina using conducting polymer modified electrodes.

Publications

1. Vini Gautam, M. Bag and K.S. Narayan; *Dynamics of Bulk Polymer Heterostructure - Electrolyte devices*; Communicated.

2. Vini Gautam and K.S. Narayan; *Conducting Polymer Coated MEAs for Enhanced Signal Recording and Stimulation*; Abstract no. 1569291840 accepted; to be published in Proceedings of 7th Intl. Meeting on Substrate Integrated Micro-electrode Arrays, 2010.

3. Vini Gautam and K.S. Narayan; *Signal and Noise Analysis of low S/N data recorded from MEAs* ; Abstract no. 1569292343 accepted; to be published in Proceedings of 7th Intl. Meeting on Substrate Integrated Micro-electrode Arrays, 2010.

4. K.S. Narayan, Vini Gautam and Monojit Bag; International Patent Application titled- *Artificial Retina Implant using Conjugated Polymers as the Photoreceptors and Transport Layers*.

List of Figures

Contents

CHAPTER 1

INTRODUCTION TO CONJUGATED POLYMERS AND THEIR INTERFACE PROPERTIES

This chapter gives a brief overview of the structure and properties of conjugated polymers. Polymers have been widely used for a long time as plastic substitutes for woods, ceramics, metals and insulation materials. However, conjugated polymers with intrinsic properties of semiconductors and metals [1] have opened up the field of Organic Electronics. The field started with the first report of high conductivity in polyacetylene on doping, by Heeger, McDiarmid and Shirakawa in 1977 [2]. Organic semiconductors and conductors have the advantage that they can be fabricated on flexible substrates and have low fabrication costs. Moreover, the electronic properties of these materials can be tuned at the molecular level.

Conjugated polymeric materials form an integral part of the work described in this thesis. The topics listed below briefly describe the concepts used to understand the observations and results in the further chapters. A detailed description of these topics can be found in various text books and reviews on organic electronics available in literature.

1.1 Conjugated polymers

Polymers are long chain organic molecules composed of repeating structural units called monomers. Conjugated polymers (CPs) are the unsaturated macromolecules

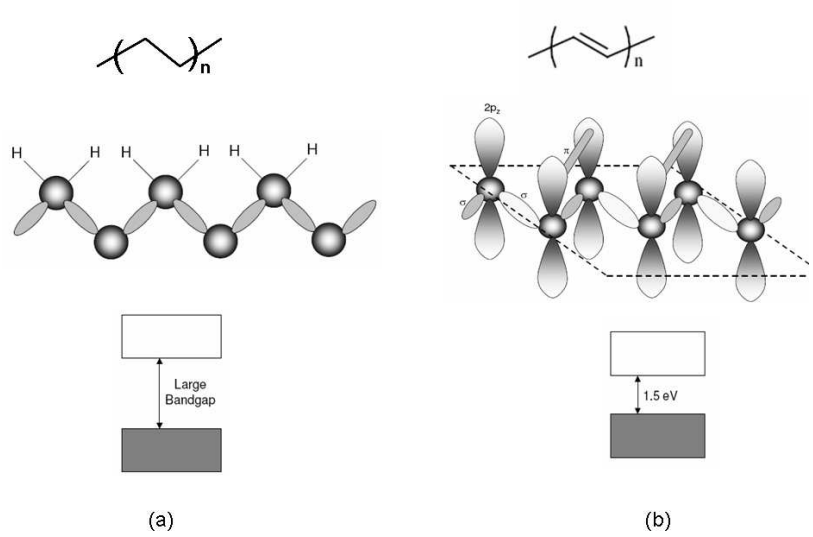

Figure 1.1: *(a) Saturated polymer poly-ethene with all σ bonds and a large band gap; (b) Unsaturated poly-acetylene with three σ and one π bond resulting in finite band gap.*

having π-electron density delocalized along the backbone chain in a quasi 1-D geometry.

In a single bonded (saturated) polymer chain like polyethylene, the ground state configuration of carbon (C) changes from $1s^2\ 2s^2\ 2p^2$ to its exited state configuration $1s^2\ 2s^1\ 2p_x^1\ 2p_y^1\ 2p_z^1$. The four outer orbitals of C atom are now equivalent and combine with four nearest neighbors by σ bonds to form a tetrahedral sp^3 hybrid structure.

According to the molecular orbital theory, two atomic orbitals overlap to form one bonding and one antibonding orbital. In ground state, the electrons occupy the bonding orbitals and determine the highest occupied molecular orbital (HOMO) or the valence band while the corresponding antibonding orbitals are empty and determine the lowest unoccupied molecular orbital (LUMO) or the conduction band. In case of the saturated polymers as described above, electron transition from HOMO to LUMO requires a large excitation energy (i.e. a large band gap exists) and

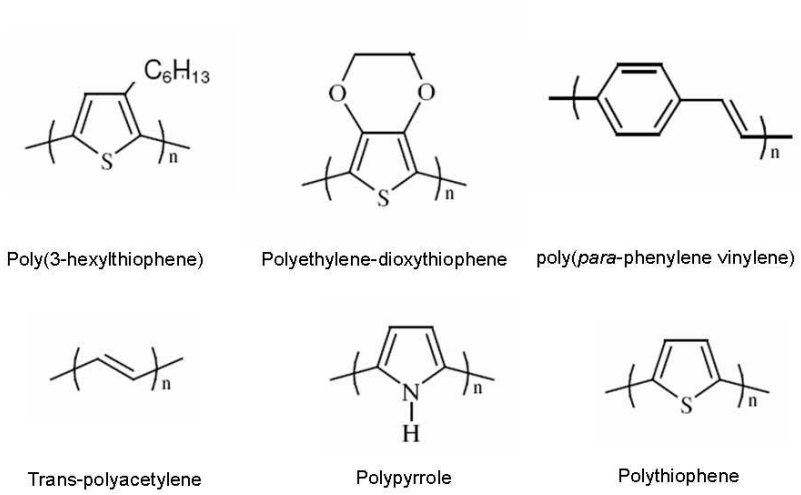

Figure 1.2: *Chemical Structures of some important conjugated polymers*

hence, these materials are insulators (Fig.1.1(b)).

In case of a conjugated polymer like polyacetylene, the exited C atom is sp^2 hybridized. Out of the four equivalent orbitals, three bind with the nearest neighbors forming two coplanar σ bonds. The remaining $2p_z^1$ orbitals of each C atom then overlap with each other to form the π bond in a direction perpendicular to the sp^2 plane. Each π bond gives rise to bonding and antibonding molecular orbitals called π and π^* respectively.

Each overlapping p_z orbital along the chain has one unpaired electron. This causes an electron delocalization along the polymer backbone where each repeating C-H unit has one π-electron. The material is therefore expected to behave like a quasi-1D metal (Fig.1.1(b)). However, there occurs a lattice distortion (dimerization) due to Peierl's instablity [3], leading to a finite band gap between the π and π^* orbitals. For most conjugated polymers, this energy gap lies in the range of 1-3eV. Consequently, these polymers behave as *organic semiconductors* and can also be optically excited. The conductivity of these polymers can be increased by *doping*. Figure 1.2 shows some common and important CPs.

1.2 Properties of Conjugated Polymers

The charge transport processes in conjugated polymers is mostly by phonon assisted hopping between localized states, which is quite different from the conventional inorganic semiconductors like Si, Ge, GaAs etc. which have highly delocalized states. Typical orders of mobility values for organic semiconductors are lower (1 $cm^2\ V^{-1}s^{-1}$) than the inorganic ones ($10^3\ cm^2V^{-1}s^{-1}$).

1.2.1 Charge Carriers

Charge carriers in conjugated polymer are interpreted as quasi-particles. These self-localized excitations arise from structural deformation over several repeating units of the polymer chain. These kind of charge carriers involve solitons, polarons and bipolarons. Charge carriers can also be generated by optical excitation. The phenomenon of photo-excitation is described in section 1.3.

1.2.2 Doping and Conducting Polymers

To increase their conductivity, conjugated polymers are doped to generate excess number of quasiparticles in the electronic structure. This doping is completely different than what is done for their inorganic counterparts. Doping here involves partial removal or addition of electrons from the polymer π-backbone using a redox reaction. Since every repeat unit is a potential redox site, oxidation (p-doping) or reduction (n-doping) can lead to a high density of charge carriers [4]. CPs can be doped by chemical and electrochemical means or by charge injection.

Following examples illustrate examples of p-type and n-type **chemical** doping in a conjugated polymer [2, 5, 6]:

(a)p-type doping

$$(\pi - polymer)_n + 3/2ny(I_2) \rightarrow \left[(\pi - polymer)^{+y}(I_3^-)_y\right]_n \quad (1.1)$$

(b) n-type doping

$$(\pi - polymer)_n + \left[Na^+(C_{10}H_8)^-\right]_y \rightarrow \left[(Na+)_y(\pi - polymer)^{-y}\right]_n + (C_{10}H_8)^0 \quad (1.2)$$

A high doping level can lead to the electronic structure of CP to be similar to that of a metal.

Both p-type and n-type doping have been obtained chemically in CPs. Generally, however, p-doping leads to more stable compounds. In the case of n-doping the dopants are alkali metals, which are unstable in air atmosphere. Furthermore, oxygen can act as an oxidant and neutralize n-doping. Even p-doping can be unstable in air if the oxidation potential of the polymer is higher [7].

Electrochemical doping of CPs involves a movement of ions into or out of the polymer structure due to a voltage applied between the CP and a counter electrode. The doping level is determined by the voltage applied. Following examples illustrate electrochemical p- and n-type doping in a CP [8–10]:

(a) p-type doping

$$(\pi - polymer)_n + \left[Li^+(BF_4^-)\right]_{soln} \rightarrow \left[(\pi - polymer)^{+y}(BF_4^-)_y\right]_n + Li_{electrode} \quad (1.3)$$

(b) n-type doping

$$(\pi - polymer)_n + Li_{electrode} \rightarrow \left[(Li^+)_y(\pi - polymer)^{-y}\right]_n + \left[Li^+(BF_4^-)\right]_{soln} \quad (1.4)$$

Examples of *conducting polymers* include polypyrroles, polythiophenes and polyanilines. While semiconducting polymers are being use in photovoltaic devices, conducting polymer forms are being extensively used for various purposes like actuators [11], electrochemical transistors [12–15], electrode-cell communications [16, 17] and electrochromics [18–22]. Their properties can be modified to suit the needs of the application. The conducting polymer : poly(3,4-ethylenedioxythiophene) (PEDOT) has been used as a conducting interface between Multi-electrode arrays and retinal tissues as described in chapter 4 of this thesis. Hence, its properties are briefly listed below.

Conducting Polymer PEDOT:PSS

PEDOT(Fig. 1.3) was originally designed to give a stable conducting polymer [23], from the point that chemical attack on the conjugated carbons (lacking the undesired α,β- and β,β-couplings) would be prevented by making a stable bond to the ether oxygen. Prepared using standard oxidative chemical or electrochemical polymerization methods, PEDOT was initally found to be an insoluble polymer yet exhibited some very interesting properties [24]. In addition to a very high conductivity, PEDOT was found to be almost transparent in thin, oxidized state [25–28]. The solubility problem was subsequently circumvented by using a water-soluble polyelectrolyte, poly(styrene sulfonic acid) (PSS), as the charge-balancing dopant during polymerization to yield PEDOT:PSS (Fig. 1.3). This combination resulted in a water-soluble polyelectrolyte system with good film-forming properties, high conductivity, high visible light transmissivity and excellent stability.

The most practically useful, polymerization method for EDT is the so-called

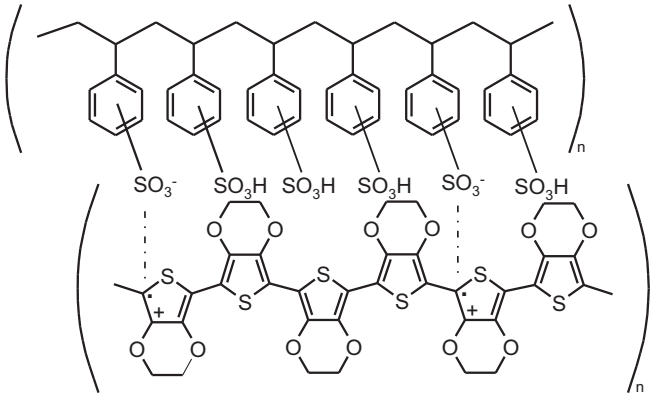

Figure 1.3: *Chemical structure of PEDOT:PSS.*

BAYTRON P synthesis that was develped at Bayer AG [29–32]. This method utilizes the polymerization of EDT in an aqueous polyelectrolyte (most commonly PSS) solution using $Na_2S_2O_8$ as the oxidizing agent. Carrying this reaction at room temperature results in a dark blue, aqueous PEDOT:PSS dispersion, which is commercially available from Bayer AG under its trade name BAYTRON P (Fig 1.3). Even after drying, the PEDOT:PSS film is highly conducting, transparent, mechanically durable, and insoluble in any common solvent [24].

Films cast from aqueous PEDOT:PSS solution have a high degree of mechanical integrity with conductivities ranging from 1 to 10 S/cm. These films are highly stable and can be treated for up to 1000 h at 100 °C with no change in conductivity. *Secondary doping* in PEDOT:PSS can be achieved by adding high-boiling point polyalcohol (sorbitol, glycerol, m-cresol, ethylene glycol). The polyalcohols aid the reorientation of the PEDOT:PSS chains to form better connections in between the conducting PEDOT chains [33]. This conformational change results in the enhancement of charge-carrier mobility in the film and leads to an enhanced conductivity by two orders of magnitude (100 - 1000 S/cm). PEDOT:PSS is a low

bandgap material, with the gap in the visible-near infrared (NIR) transition region and shows an absorption maximum in the middle of the visible spectrum at 2.2 eV (600 nm).

PEDOT:PSS has been extensively studied as the active material in lateral electrochemical diodes, triodes and transistors [34], as the charge injecting and extracting layer in organic light-emitting diodes [35] and organic solar cells [36], and as electrodes in organic field-effect transistors [37] and for various sensing activities.

1.2.3 Charge Transport

There are many proposed models to explain conduction mechanism in conjugated polymer based systems. The semi-classical approach of periodic potentials and Bloch waves explains the well defined band structure of crystalline solids. However, in amorphous and disordered systems, impurities and lattice defects introduce 'Anderson Localization', i.e. the wave functions become localized and energy states appear within the band gap of these systems [38].

Disordered systems like conjugated polymers can be thought of as a electronic wires broken into subunits by chemical or physical defects where the subunits act as the conjugation unit and determines the conjugation length. Therefore a localized distribution of sites is obtained that hold charge. These sites are spread in real space as well as energy space, i.e carriers get spatially and energetically localized. As a result, the material should behave like an insulator. However, the localized charge carriers travel through the material by **hopping** from one localized state to another. The rate of hopping determines the conductivity and mobility of carriers.

Miller and Abraham proposed a hopping model in conjugated polymers based on *phonon assisted quantum mechanical tunneling* and gave an expression for charge carrier transition rate from one site(i) to another(j) [39]. They showed that the probability of a carrier to hop depends on both the height of the barrier (activation energy) as well as the spatial distance r between the two sites:

$$\Gamma = \nu_{ph} \exp(2\gamma|r_{ij}|)\{\exp -\frac{\epsilon_j - \epsilon_i}{k_B T} \quad when \quad \epsilon_j > \epsilon_i; \quad 1 \quad otherwise\} \tag{1.5}$$

Here, ν is the phonon vibration frequency, γ is the inverse localization radius, k_B is the Boltzmann constant and T is the temperature.

Based on similar phonon effects, Mott later proposed a *variable range hopping (VRH) model* [40]. Mott's theory is based on the notion that charge transfer will take the fastest route from one site to the other. He proposed that carriers may either hop a small distance with high activation energy (energetic distance between the sites), or a long distance with low activation energy.

Variable range hopping mechanism can be used to empirically describe the temperature dependence of conductivity for lightly to moderately doped conjugated polymers.

1.2.4 Trap States

As discussed above, charge transport properties of organic semiconductors are strongly affected by traps since trapped charge carriers can not take part in transport. Trap states are those localized energy states within the energy gap of the semiconductor where charge carriers get captured in. Such trapped carriers are either released after a retention period or they get recombined with carriers of opposite charge sign. The columbic charge on these states influences the electric field

distribution in a device and hence the transport. For instance, this can cause a delay and hysteresis effects in alternately operating devices [41].

Sources for origin of trap states can be:

- Impurities : If the HOMO or LUMO of an incorporated molecule lies within the gap of the host molecule, then it acts as a trap.
- Structural Defects : Structural imperfections lead to a wide distribution of HOMO/LUMO levels out of which a few states act as trap states.
- Geminate Pairs : Organic solids have strong columbic interactions due to the low dielectric constant. A hole and electron can be bound columbically even if several molecules separate them. Such a pair is called a geminate pair and forms a Coulomb trap. Such traps occur when both the types of charge carriers are present.

1.3 Photogeneration of Charge Carriers

The application of semiconducting conjugated polymers in photovoltaic devices like OLEDs and OFETs is entirely based on the mechanism, extent and mobility of the photogenerated charge carriers. As discussed before, the band gap of most semiconducting polymers lie in the range 1-3 eV and hence, they can be excited by visible-near infrared photons. Absorption of a photon leads to the formation of electron-hole pair. If this electron-hole pair remain on the same chain with electron and hole bound to each other by electrostatic forces, the pair is called an **exciton**, defined as quasiparticle consisting of electron-hole pair of finite binding energy. The binding energy lies in the range $\sim 0.4 - 1$ eV [42]. Photoinduced charge transport in semiconducting polymers is through the following route: (i) exciton formation,

(ii) exciton diffusion, (iii) exciton dissociation into positive and negative charge carriers and finally (iv) transport of majority charge carriers under the influence of applied electric field.

Formation of excitons: As mentioned above, excitons are formed upon photoexcitation.

An exciton, being electrically neutral, does not contribute to the charge transport but it transports the energy from one site to the other depending on the diffusion length ($\sim$ several nm). The extent of delocalization of excitons strongly depends on the interplay between intermolecular interactions and the Coulomb interactions. Excitons can be classified as:

- *Intrachain excitons* are composed of electron-hole pair in a single chain within the same conjugation element and predominantly appeared in polymer systems.
- *Interchain/Charge-transfer excitons* are the species in which electron and hole belong to two different molecules or two different polymeric chains with different bandgap energies.

Transport of excitons: Although excitons are initially localized on a single molecule and electrically neutral, these quanta of energy can travel through the solid even up to several hundreds of molecules away from the source of creation. These quasiparticles normally transport the energy without the migration of net electric charge. The transport may be either *radiative* in which an exciton emits a photon that is absorbed by another part of the solid to create a second exciton, or *non-radiative* like electromagnetic wave packet transport,

hopping transport and long-range resonant transfer through the distribution of exciton.

Exciton Dissociation: The created exciton has two fates during its temporal evolution. The exciton can eventually separate and escape from recombination. This contributes to the photocurrent. The probability is termed as quantum yield or sometimes *quantum efficiency* (η), by definition, the amount of free charges collected per single photon absorbed. The other possibility is that exciton may recombine, which results in fluorescence (radiative recombination) or an increase in thermal energy of the medium (non-radiative recombination).

Excitons can be dissociated by either thermal energy or electric field or both. In conjugated polymers, the value of typical exciton binding energy lies in the range of $E_{exc} \sim 0.4$ - 1 eV. To compensate the binding energy, one may need several thousand degrees of Kelvin, which is not a reasonable option. Another way to dissociate exciton is to apply external electric field $E_{ext} > (E_{exc}/er_{exc})$. For a conjugated polymer, the exciton radius r_{exc} is of the order of 1 nm, yielding minimum field required $\sim$ 106 V/cm.

1.4 The Bulk Heterojunction System

The origin of bulk heterojunction lies in the use of conjugated polymers in photovoltaic (PV) devices. The first photovoltaic cells in 1950's were made of crystalline silicon. Practically all conventional inorganic solar cells incorporate a doped semiconductor to form a p-n junction across which photo-voltage is generated. In the region near the junction, an electric field is formed and the electrons and holes generated by light absorption in the bulk Si diffuse to this junction where they are

directed by the electric field towards the proper electrode. Over the years, solar cells have been made from many other semiconductor materials with various device configuration such as single-crystal, polycrystalline, and amorphous thin-film structures.

Organic semiconductors are a less expensive alternative to inorganic semiconductors like Si. Moreover, compared to Si, they can have extremely high optical absorption coefficients that offer the possibility for the production of very thin solar cells. They can be easily fabricated on flexible plastic substrates in an easily scalable high-speed printing process and can reduce the balance of system cost for organic PVs.

The exciton diffusion lengths in organic devices are typically 1-10 nm, [43–45] which is much shorter than the device thicknesses. Exciton diffusion limits charge-carrier generation in these devices because most of them are lost through recombination. Photogeneration is therefore a function of the available mechanisms for *excitons dissociation*. A major breakthrough in cell performance came in 1986 when Tang discovered that much higher efficiencies (about 1%) can be attained when an electron donor (D) and an electron acceptor (A) are brought together in one cell [46]. This **heterojunction** concept is at the heart of all three types of organic PV cells that currently exist: dyesensitized solar cells; planar organic semiconductor cells; and high surface area, or bulk heterojunction (BHJ) cells.

The idea behind a heterojunction is to use two materials with different electron affinities and ionization potentials. At the interface, the resulting potentials are strong and may favor exciton dissociation: the electron will be accepted by the

material with the larger electron affinity and the hole will be accepted by the material with the lower ionization potential, provided that the difference in potential energy is larger than the exciton binding energy. In the planar heterojunction, or bi-layer device, the organic D/A interface separates excitons much more efficiently than an organic/metal interface in the single layer device.

In this device the excitons should be formed within the diffusion length of the interface. Otherwise, the excitons will decay, yielding, e.g., luminescence instead of a contribution to the photocurrent. Since the exciton diffusion lengths in organic materials are much shorter than the absorption depth of the film, this limits the width of effective light-harvesting layer in such devices.

In a dispersive (or bulk) heterojunction, the donor and acceptor material are *blended* together [47–49]. If the length scale of the blend is similar to the exciton diffusion length, the exciton decay processes is dramatically reduced since in the proximity of every generated exciton there is an interface with an acceptor where fast dissociation takes place. Hence, charge generation takes place everywhere in the active layer. Provided that continuous pathways exist in each material from the interface to the respective electrodes, the photon to-electron conversion efficiency and, hence, the photosensitivity is dramatically increased.

Semiconducting polymers and molecules combine the optoelectronic properties of conventional semiconductors with the excellent mechanical and processing properties of plastic materials. Additionally, they possess an unprecedented flexibility in the synthesis, allowing for alteration of a wide range of properties, such as bandgap, molecular orbital energy level, wetting and structural properties, as well as doping.

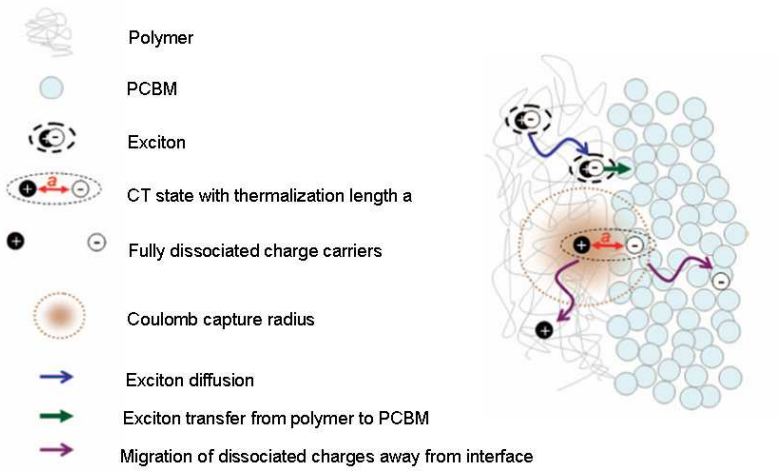

Figure 1.4: *Schematic of a donor/acceptor interface showing the processes in a BHJ device [51].*

Because luminescence quenching and ultrafast photoinduced electron transfer from a conjugated polymer (as donor) to buckminsterfullerene(C_{60}) or its derivatives (as acceptor) had already been observed [50], this material combination has been extensively studied in bulk heterojunction PV cells.

In 1995 Yu et al. [47] fabricated the first fully organic BHJ cell which was based on a mixture of soluble p-phenylene vinylene (PPV) derivative with a fullerene acceptor. The attention has now been shifted towards polymer:fullerene (like PCBM) BHJ solar cells based on polythiophene derivatives as absorbing and electron donating material [52–54]. By optimizing the processing conditions, efficiencies in excess of 4% have been reported for solar cells based on these material systems.

The fundamental physical processes in a BHJ device with PCBM are schematically represented in an energetic diagram as depicted in Fig. 1.4. Sunlight photons which are absorbed inside the device excite the donor, leading to the creation of excitons in the conjugated polymer. The created excitons start to diffuse within

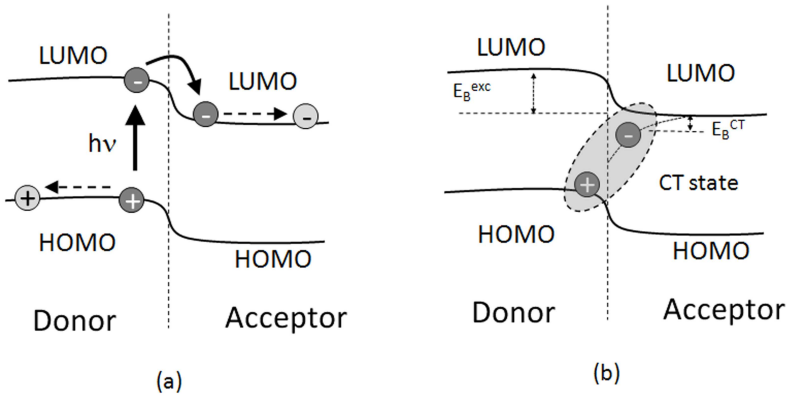

Figure 1.5: Energy level diagram of a donor/acceptor interface (a)Photoexcitation in donor HOMO followed by e transfer in acceptor LUMO and migration towards the electrodes. (b) Interfacial e−h pairs forming the charge transfer (CT) states.

the donor phase and if they encounter the interface with the acceptor then a fast dissociation takes place leading to charge separation. The resulting metastable electron-hole pairs across the D/A interface may still be coulombically bound and an electric field is needed to separate them into free charges. Subsequently, the separated free electrons(holes) are transported with the aid of the internal electric field, caused by the use of electrodes with different work functions, towards the cathode (anode) where they are collected by the electrodes and driven into the external circuit [55].

Figure 1.5 shows the band diagrams and the interfacial energies in a BHJ device. E_B^{exc} is the coulomb binding energy of the exciton. Since the donor and acceptor are quite close to each other, the charge separation is only modest even after the transfer to the acceptor. The e and h still exhibit a significant Columbic attraction comparable to thermal energy and represents a barrier to charge photogeneration in at D/A organic interfaces [56].

A bulk heterojunction system (of a thiophene derivative and an acceptor type polymer) in contact with a liquid electrolyte has been studied in the next chapter. To understand the mechanisms of charge transfer at the interfaces of such an organic polymer-liquid electrolyte interfaces, a relevant background of the band structures of semiconductor-electrolyte interfaces is necessary. Such interfaces have been primarily studied for inorganic semiconductors like silicon. Organic semiconductor-electrolyte interfaces are expected to show different characteristics. The following section briefly includes some of the related topics.

1.5 Semiconductor-Electrolyte Interface

The interface between a metal and an electrolyte behaves like a capacitor. The excess charge on the metallic electrode is like a surface charge separated from the ionic counter charge in the electrolyte by the distance of a solvation shell. This structure is referred as the Helmholtz double layer. The Helmholtz capacitance is denoted by C_H. In dilute solutions, the counter charge in the electrolyte can be extended over a space charge range which is modeled by the Gouy-Chapman theory. In some cases, few ions can come closer to the surface by chemisorption, losing part of their solvation shell in this process. This led to the Sterns model for the influence of specific ion adsorption on the double layer structure and capacity.

Unlike metals, a diffuse space charge layer exists in the in the semiconductor side as well. If the electrode is a semiconductor with moderate conductivity, this space charge layer can dominate the whole capacitance behavior of the electrode. The three typical situations found at an n-type semiconductor in its space charge layer are shown in (Fig. 1.6). Briefly, following are the possible features of the interface:

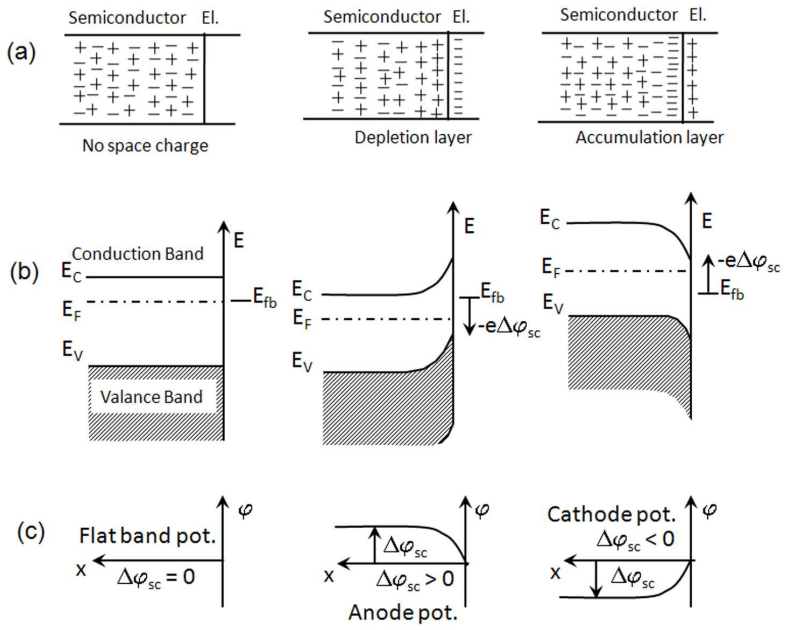

Figure 1.6: *Schematic showing the space charge layers in an n-type semiconductor in contact with an electrolyte. (a) Distribution of charge carriers; (b) Course of band edges (c) Course of electric potential. Redrawn from [57].*

1. The interface without an excess charge on the semiconductor occurs at the potential of zero charge (pzc) for the electrode. At the pzc, the bands are flat. This is the so-called flat-band potential. The positive charge of the immobile donor states in the semiconductor is compensated by the negative charge of the mobile electrons.

2. The case when the positive excess charge from donors in the semiconductor get compensated for by a negative counter charge at the interface from ions in the electrolyte. The space with the positive charge is depleted of electrons (depletion layer). The positive excess charge in the depletion layer extends into space, causing the bending of the band edges downwards from the interface.

3. Figure also shows the case where the semiconductor has a negative excess charge of electrons which are accumulated near the interface, compensated by a positive charge of ions at the interface (accumulation layer). The negative excess

charge situation has a much smaller extension into space and results in an upward band bending.

4. The inversion layer is formed when the Fermi level at the electrode interface approaches the band edge level of mobile minority charge carriers with increasing potential across a depletion layer. Since the minority charge carriers are accumulated in the inversion layer, the interfacial property changes from the n-type to the p-type property or from the p-type to the n-type property as a result of forming an inversion layer.

5. The deep depletion layer is formed as an extension of a depletion layer not leading to an inversion layer but producing an insulating layer in which no minority charge carriers are accumulated because the minority charge carriers is prevented from transferring between the interface and the interior of semiconductor. In both depletion and deep depletion layers the charge is carried by immobile ionized donors and acceptors.

A useful way of measuring the charge distribution at the interface is to measure differential capacitance. The differential capacitance of a semiconductor-electrolyte interface can be represented by a series of three capacitances, as shown in Fig. 1.7.

This figure also shows the differential capacitance dependence on the voltage drop in the individual capacitors. The measured voltage drop consists of the sum of these three voltage drops. Since in a series of capacitors the overall capacitance is determined by the smallest one, it is clear that, in the range of positive voltages, the total capacity is determined by the space charge capacity of the n-type semiconductor, since this is by far smaller than the other two capacitances. The capacity of the diffuse double layer can only play a role very close to the pzc. In concentrated

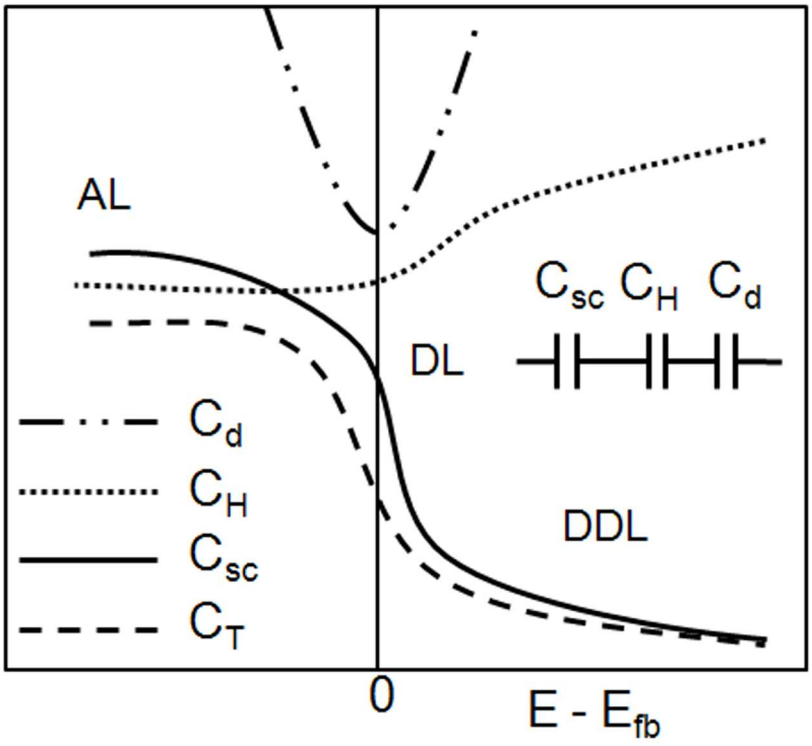

Figure 1.7: *Schematic showing the behavior of space charge capacitances of an n-type semiconductor as a function of bias. C_{sc} is the space charge capacity of the semiconductor, C_H is the Helmholtz layer capacitance, C_d is the capacitance of the diffuse layer of charges in the electrolyte and C_T is the total capacitance. E_{fb} is the flat band potential of the semiconductor and E is the applied bias. AL, DL and DDL represent the accumulation, depletion and deep depletion regimes of the space charge capacitance respectively. Redrawn from [57].*

electrolytes, this contribution can be neglected. For a p-type semiconductor the situation is reversed with respect to the polarity of the voltage applied.

The utility of both the undoped and doped states of conjugated polymers have been demonstrated in the research work presented in this thesis. In the following chapter, conjugated polymers in pristine form and in bulk heterojunction form have been studied in contact with an electrolyte. Chapter 4 uses the doped, conducting form of a conjugated polymer. It should be noted that the application described in chapter 4 is a non-conventional subject area. Therefore, a brief but relevant background of the important topics is provided in chapter 3.

CHAPTER 2

PHOTO-VOLTAGE AND PHOTO-CAPACITANCE STUDIES ON SEMICONDUCTING POLYMER-ELECTROLYTE INTERFACE

2.1 Motivation

Several electrochemical processes occur when a semiconductor establishes a contact with an electrolyte. Charge transfer reactions and formation of electrical double layers dominate these processes. Inorganic materials like Silicon, Germanium and GaAs are well studied for their interfaces with electrolyte solutions because of their use as electrodes in photo-voltaic and catalytic cells. The key areas of study have been charge transfer reactions at the interfaces [58], excited electronic states and reactivity [59], surface corrosion and passivity [57, 60, 61], chemical sensing [62], impedance spectroscopy [63] and luminescence and electro-reflection [64, 65].

Conjugated polymer-electrolyte interfaces are important from the perspective of their increasing use in devices such as polymer electrochemical photovoltaic cells and electrolyte-gated organic field effect transistors. Organic semiconductors have been shown to be stable in presence of electrolytes and sizable optoelectronic changes have been observed in these devices [66]. There have also been a few reports on impedance measurements of these devices [67, 68].

However, there have been no studies related to these interfaces at high frequencies (ω >10 kHz). High operating frequencies require fast switching times of the device. The presence of interfacial capacitances however, can be a limiting factor

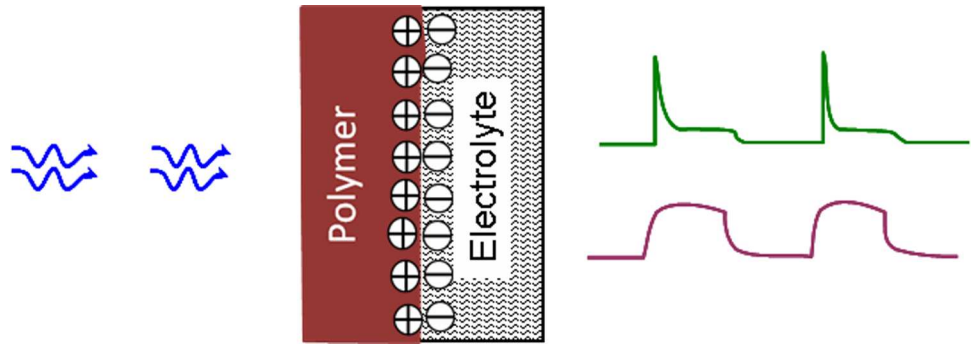

Figure 2.1: *Schematic showing response of a polymer-electrolyte device for a pulse light input.*

for such applications as the charge kinetics can become limited due to the ions in the electrolyte. High frequency studies are also important to study the fundamental nature of transport within these devices.

This chapter summarizes the experiments done on *metal-organic semiconductor-electrolyte* device geometry under photo-illumination. In the first section, experiments related to the transient **photo-voltage** are described with n-, p- and blend-type polymer on different substrates. The second section describes experiments involving **photo-capacitance** and C-V measurements at low as well as high frequencies.

2.2 Materials used

Both the voltage and capacitance measurements were done on P3HT, N2200 and P3HT/N2200 blend systems.

- P3HT (Poly(3-hexylthiophene)): is an alkyl substituted thiophene compound and is optically active. It is obtained in powder form from Aldrich Chem. Co. and is regioregular. Its HOMO level lies at 4.9 eV and LUMO at 2.7 eV.

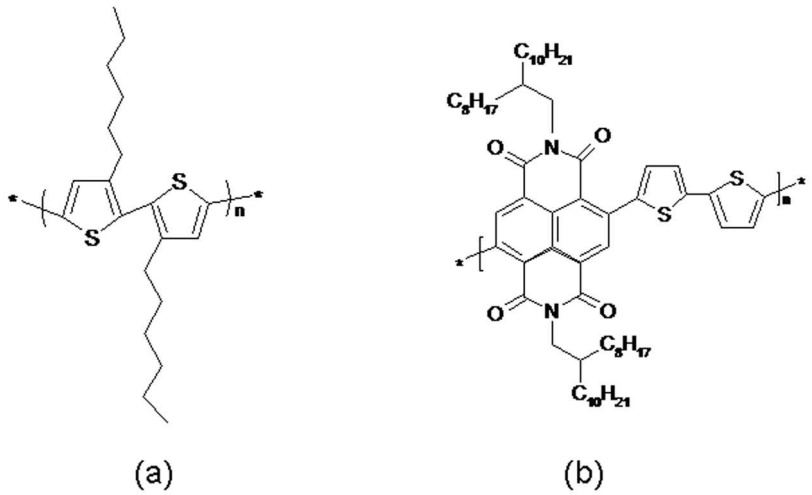

Figure 2.2: *Chemical structure of (a)P3HT and (b)N2200.*

Absorption maximum lies at 560 nm. P3HT is mainly an donor type (hole transporting) organic semiconductor.

- ActivInk N2200: is a NDI-based polymer poly[N,N'-bis(2-octyldodecyl)- naphthalene-1,4,5,8-bis(dicarboximide)-2,6-diyl]-alt-5,5'-(2,2'-bithiophene), (P(NDI2OD-T2), obtained from Polyera Co. Its HOMO level lies at 5.36 eV and LUMO level at 3.91 eV and absorption maximum at 391 nm and 697 nm. It is an acceptor type (electron transporting) organic semiconductor and has recently been reported the most stable n-type organic semiconductor [69].

- P3HT/N2200 (blend): is a bulk heterojunction system where P3HT acts as the donor and the n2200 as the acceptor. It is made by dissolving P3HT and N2200 in chlorobenzene in 1:1 ratio by weight. The chemical structures of P3HT and N2200 are shown in Fig. 2.2.

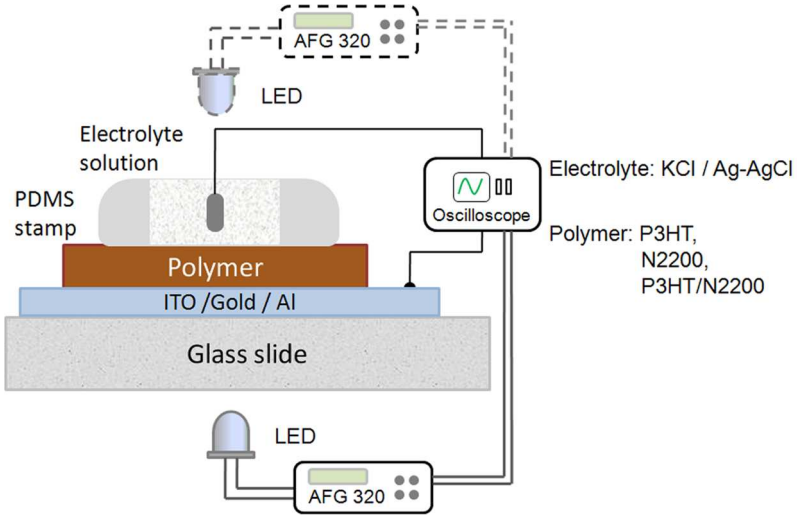

Figure 2.3: *Experimental set-up for measuring photovoltage.*

2.3 Photo-voltage Measurement

2.3.1 Experimental set-up

The polymer/electrolyte device schematic is shown in Fig. 2.3. Following are the details of the methods and set up:

- P3HT and N2200 were used without any additional purification. Chlorobenzene was used as the solvent (20 mg/ml concentration) and the solution was spin cast on the electrode-glass substrates. The polymer coated substrates were annealed for 15 min at 80 ^{o}C. Thickness of the films could be varied by changing the speed (rpm) of the spin coater. All procedures were done inside the glove box.

- Two kinds of bottom electrodes were used : Indium tin oxide (ITO, 20 ohm/sq) and gold. Gold substrates were prepared by vapor depositing gold in the thermal evaporation chamber on pre-cleaned glass slides.

- KCl solution (100 mM) was used as the electrolyte. PDMS wells were made

to hold this solution on top of the polymer films.

- Ag/AgCl pellet was used as the top electrode (from Warner Instruments).
- LEDs were used as light sources and their waveforms were controlled using a Function Generator (Sony Tektronics AFG320).
- Direction of photo-illumination was from either side : polymer-electrode side (bottom illumination) or polymer-electrolyte side (top illumination).
- Oscilloscope (LeCroy Waverunner 6100A) was used to record the photo-voltage at a sampling rate of 250 kS/sec.

The experimental results can be explained on the basis of the energy bands of the polymer systems, the work functions of the metal electrodes and the redox potentials of the electrolyte. The relative positions of these levels are shown in Fig. 2.4.

2.3.2 Variation of photo-voltage with the type of polymer and the metal electrode

Observations

The photo-voltage response of P3HT, N2200 and P3HT:N2200 blend films on gold and ITO substrates is shown in Fig. 2.5. The polymer films were considerably thick (> 0.4 μm). 100 mM KCl was used as electrolyte on top of the polymer.

It was observed that the photo-voltage response of the polymer systems on gold and ITO are quite different. Moreover, the direction of illumination also makes a difference in the photo-voltage response. The photo-excitation leads to a generation of charge carriers largely at the polymer-electrode interface in case of illumination

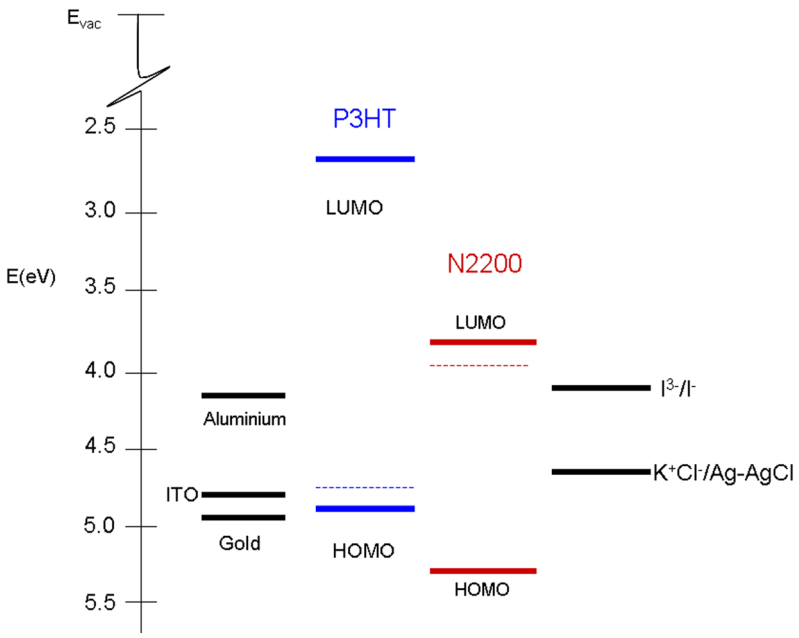

Figure 2.4: *Work functions of the materials used and their relative positions w.r.t. vacuum level. The schematic does not represent the exact device.*

from the electrode side and at polymer-electrolyte interface in case of illumination from the electrolyte side (as shown in Fig. 2.3). The response across the metal-electrolyte device will therefore depend on the bulk mobilities of charge carriers diffusing to the other interface.

Analysis

(a) P3HT is a donor-type polymer and its fermi level lies close to the HOMO (4.9 eV). Work functions of ITO and gold are close to 4.8 eV and 5.1 eV respectively. Therefore, the P3HT band is close to the ITO or gold electrode and hence the contact is fairly ohmic at the metal interface. At the other interface of P3HT, the effective redox potential of Ag/AgCl in 100 mM KCl is around 4.6 eV. Hence, the bands at this interface bend downwards to maintain equilibrium between the fermi level and the redox potential (Fig. 2.6(b)).

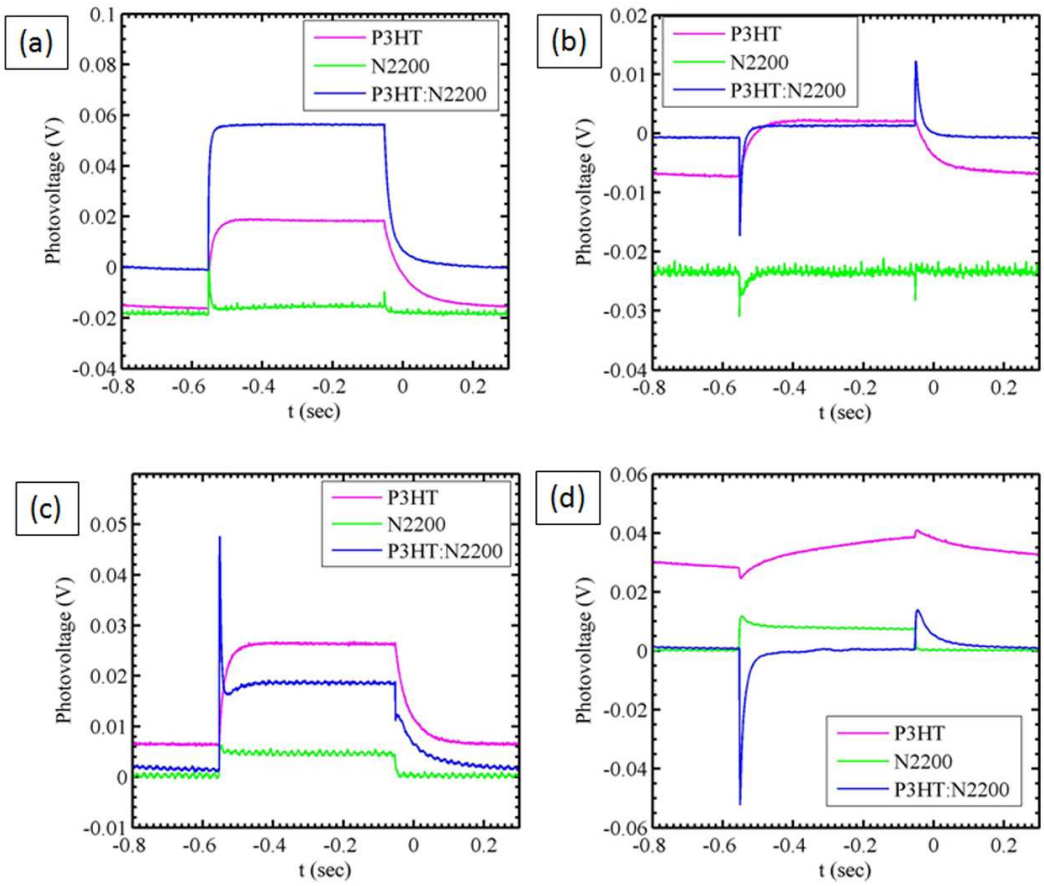

Figure 2.5: *Photovoltage from P3HT, N2200 and blend with gold as the bottom electrode (a) Top Illumination (b) Bottom Illumination and with ITO as the bottom electrode (c) Top Illumination (b) Bottom Illumination. The duration of light pulse is 500 ms.*

Upon photo-illumination from the polymer-electrolyte side on reasonably thick samples, the absorption is largely restricted to the volume of polymer beneath the electrolyte. Therefore, the charges (electrons and holes) are generated primarily at the polymer-electrolyte interface. The excited electrons get transferred from the LUMO of P3HT to the electrolyte (built-in-field assisted transport) while the holes are transported from the HOMO to the gold or ITO electrode at the other interface. The response is therefore a positive DC photo-voltage from both gold and ITO electrode contacts (Fig. 2.5(a) and (c)).

Illumination from the electrode-polymer side generates electrons and holes largely in the volume of polymer close to this interface. But there is a difference in the photo-voltage generated on gold and ITO electrodes. The photogenerated holes are readily transferred to the gold electrode resulting in an initial rise in potential; but since bulk mobility of electrons, μ_e, is less through P3HT, the steady state photo-voltage is not established across the device (Fig. 2.5(b)) Moreover, when P3HT is in contact with ITO, band bending is more and some of the excess photogenerated electrons can get collected by the ITO electrode. This phenomenon results in a drop in photo-voltage at the onset of excitation, followed by a slow rise in steady state potential due to low bulk mobilities of electrons (Fig. 2.5(d)). Because gold has lower work function than ITO, the tunneling probability of electrons to gold is less and hence the drop in photo-voltage is not seen.

(b) N2200 is an acceptor-type polymer with its fermi level close to the LUMO (3.9 eV). In this case, the work functions of both ITO / gold as well as electrolyte system are less than the fermi level of the polymer. Thus, in dark, the energy

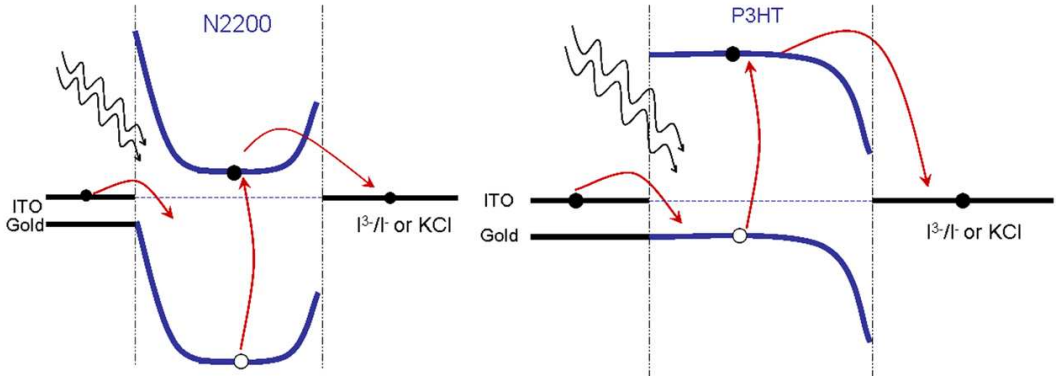

Figure 2.6: *Band diagrams of P3HT and N2200 films between a metal electrode and an electrolyte. This diagram is not drawn to scale. The dark circles represent electron and white circles represent hole.*

bands of the polymer are bent upward at both the interfaces. However, the band bending is more towards the ITO / gold electrodes (Fig. 2.6(a))

Upon photoexcitation from the polymer-electrolyte side for N2200 thick films, the photo-generated charge carriers are generated primarily at the polymer-electrolyte interface. Due to the lower energy barrier at the electrolyte interface, the electrons get transferred to the electrolyte while the holes travel through the polymer bulk towards the bottom ITO or gold electrode. Hence the response from N2200 is a positive transient voltage at the onset of photoexcitation followed by almost zero DC potential. This result was found to be consistent for both the gold and ITO bottom electrodes (Fig. 2.5(a) and (c,d)).

Upon illumination from the polymer-electrode side, the photo-generated holes are readily transferred to the bottom ITO and electrons are transported towards the electrolyte; resulting in a positive steady state photo-voltage. However, due to an initial electron transfer to gold, there exists a drop in the photo-voltage at the onset of excitation (Fig. 2.5(b)).

(c) The blend system of P3HT:N2200 is a bulk heterojunction system which shows a photo-voltage response that has features of both P3HT and N2200 semiconducting polymers (Fig. 2.5).

As observed from the above results, the photo-voltage response of a thick film has considerable contribution from the polymer bulk. It is expected that the response of a comparatively thin film of the same polymer would be primarily dominated by its interfaces on either side. The following section includes the observations of photo-voltage response measured with thin films.

2.3.3 Variation of photo-voltage with thickness of polymer film

These experiments were done with the blend system. The bottom electrode was ITO. Thickness was varied by changing the concentration of the polymer or by changing the speed of spin casting. White light was used for illumination.

Observations

The results are shown in Fig. 2.7. For a reasonable thick film (4.5 μm), illumination from the polymer-electrolyte side leads to a positive photo-voltage spike followed by a slow drop to a steady value (Fig. 2.7(a)). With reducing thickness, the ratio of photo-voltage spike height to its steady value reduces. As shown in Fig. 2.7(b), when the thickness is reduced to 0.2 μm, there is an initial sign reversal of the photo-voltage spike, then the steady state value is positive. Thus, as the thickness is reduced from 400 μm to the order of 0.2 μm (200 nm), the photo-voltage reverses its sign at the onset of photoexcitation.

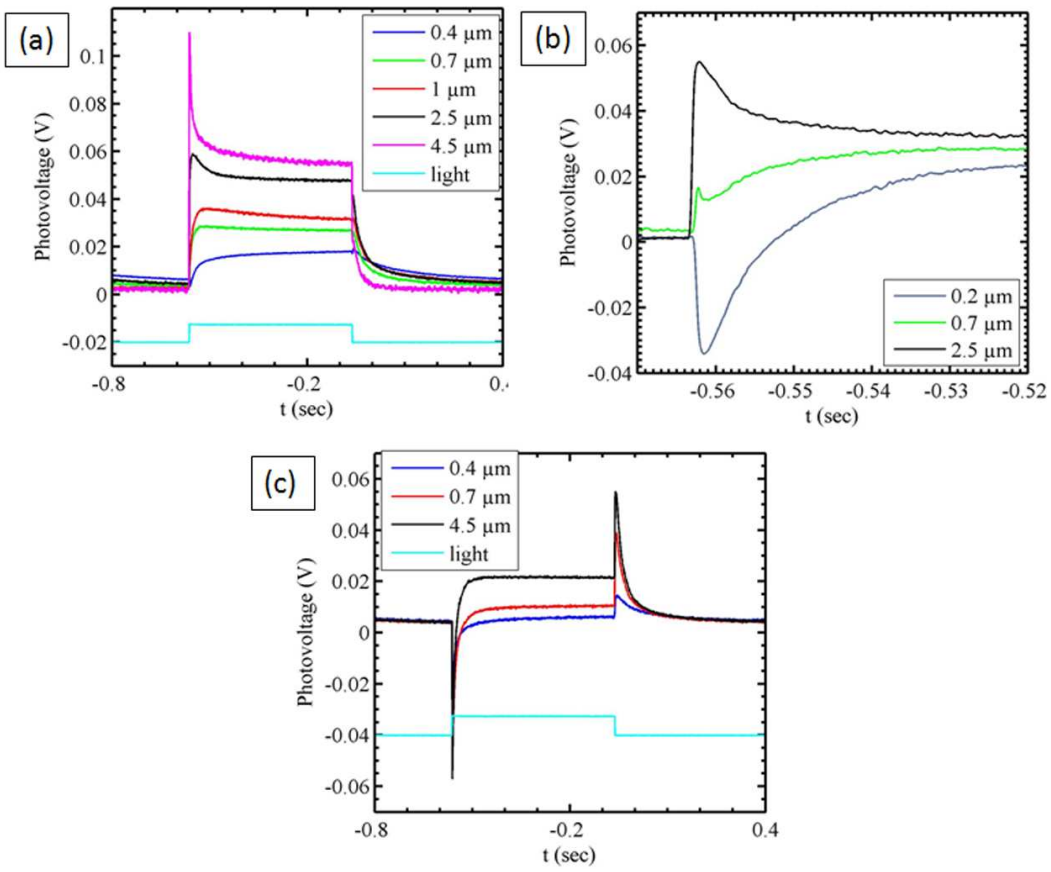

Figure 2.7: *Photovoltage from P3HT:N2200 blend films on ITO bottom electrode as a function of film thickness (a) Top Illumination (b) The initial transient is shown in zoom scale. Duration of light pulse is 500 ms. (c) Results for the same sample when illuminated from bottom.*

Analysis

The rate of generation of electrons and holes differ in a blend with both donor and acceptor type polymers. Photo-excitation from the polymer-electrolyte interface on a thick film (4.5 μm) leads to an immediate and fast transfer of generated electrons to the electrolyte leading to the initial positive spike of photo-voltage. This is followed by a steady state potential due to the collection of holes by the bottom electrode. The opposite phenomenon takes place when the same sample is illuminated from the polymer-electrode side (Fig. 2.7(c)). In this case, the charge carriers are predominantly generated in the vicinity of the electrode. Thus, electrons get collected by the electrode while holes get collected by the electrolyte, leading to a negative spike.

As the film thickness reduces to 200 nm, the charge carriers are generated on both polymer-electrode and polymer-electrolyte interface. The electron transfer to the electrode followed by the holes is the dominating process. Therefore, for a considerable thin film, irrespective of the direction of illumination, the photo-voltage is initially negative and then positive in the steady state.

2.3.4 Photo-voltage vs. wavelength and intensity of excitation

Blue, white and red LEDs were used as light sources.

The rate of photogenerated carriers is given by the following equation:

$$G(x, \lambda) = \alpha(\lambda) I_o e^{-\alpha(\lambda)x} \tag{2.1}$$

Here, α is the light absorption coefficient which is a function of wavelength of light and I_o is the intensity of incident light. Hence we expected the photo-voltage

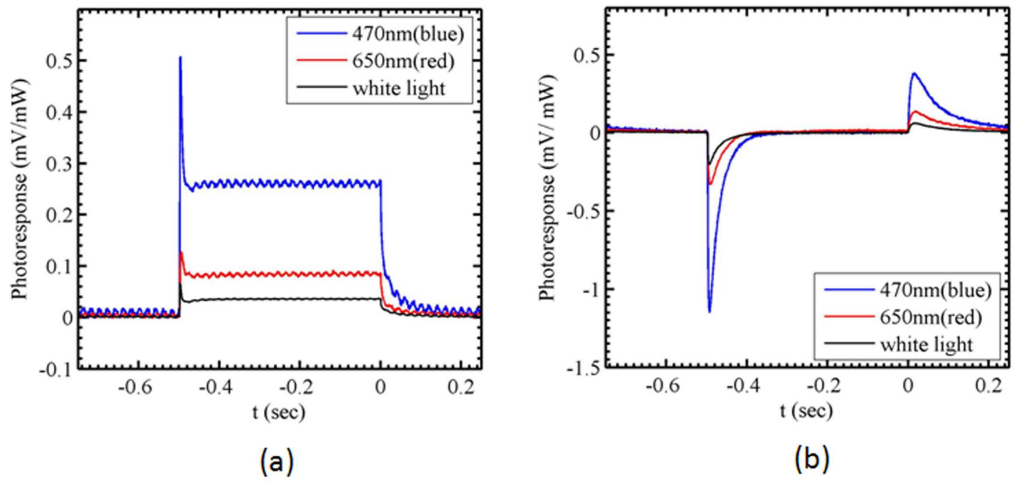

Figure 2.8: *Photovoltage from P3HT:N2200 blend thick film on ITO bottom electrode for blue, red and white LEDs driven at same voltage for 500 ms duration. (a) Top illumination (b) Bottom illumination*

signal to vary with incident wavelength and intensity.

Thus, higher the intensity of illumination, more the rate of charge generation. Moreover, penetration depth, L_p, is equal to α^{-1} and is directly proportional to the wavelength of light. Thus, red light will have greater penetration inside a thick sample than blue light. In other words, blue light is more absorbed than red.

Observations

The intensity and wavelength (color) dependence of photo-voltage is shown in Fig. 2.8 and 2.9 respectively. We observe from the plots that the time constants for rise and fall of the photo-voltage are a function of intensity of the incident light. Also, the response from blue light is more than the red light.

Analysis

Before getting transferred to the electrolyte, the charge carriers generated in bulk can either get trapped at the surface states or, recombine before reaching the

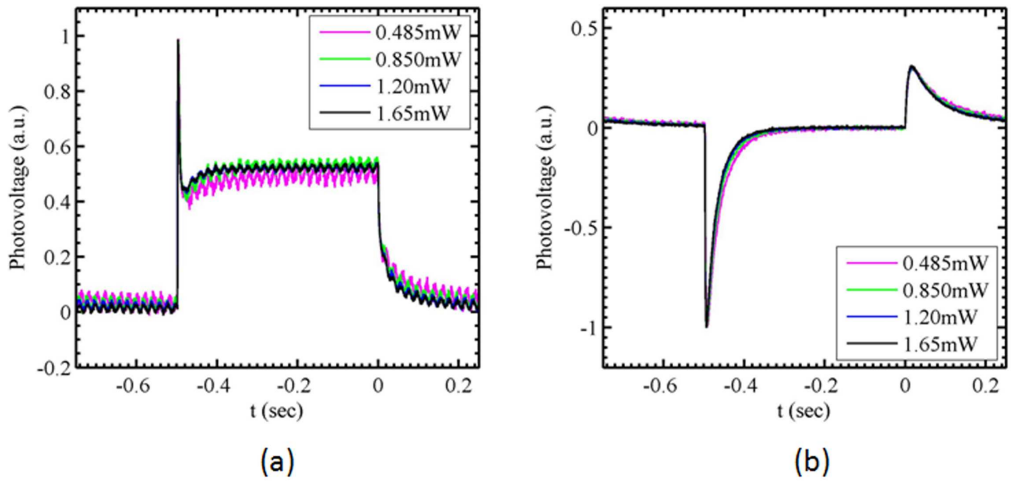

Figure 2.9: *Photovoltage from P3HT:N2200 blend thick film on ITO bottom electrode for white light illumination at different intensities. Note the variation in time constants as a function of intensities for both rise and fall of the photovoltage. (a) Top Illumination (b) Bottom Illumination*

polymer-electrolyte junction. For blue light, the charges are generated within the space charge region and are therefore readily transferred to the electrolyte under the space charge field *drift*. For red light, however, the penetration depth is more than the width of the space charge region. The holes or electrons generated deep in the bulk usually suffer recombination due to less *diffusion* lengths. Hence, the signals are more for blue than red light.

2.4 Photo-capacitance Measurements

The distribution of electric charges at the semiconductor - electrolyte interface can be observed by measurement of the interfacial capacitance. The total capacitance across the metal-semiconductor-electrolyte device is the net sum of capacitance of space charge on the semiconductor side (C_{sc}), the Helmholtz layer at the interface (C_H) and the diffuse layer on the electrolyte side, when the metal contacts are ohmic (Fig. 3.2). The net capacitance (C_T) is therefore smaller than the least

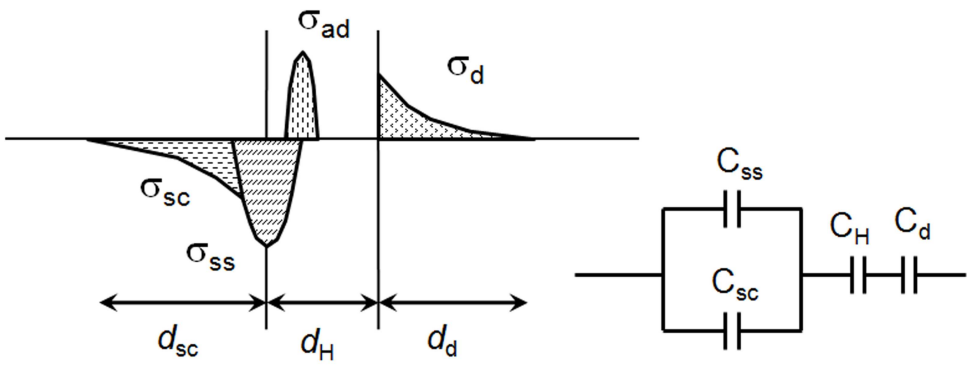

Figure 2.10: *Equivalent circuit for a semiconductor-electrolyte system showing the capacitances involved. C_{sc} is the space charge capacity of the semiconductor, C_{ss} is the capacitance of surface states, C_H is the Helmholtz layer capacitance and C_d is the capacitance of the diffuse layer in the electrolyte. The resistances for leakage pathways are not shown.*

value of either of the three capacitances, and is given by:

$$\frac{1}{C_T} = \frac{1}{C_{sc} + C_{ss}} + \frac{1}{C_H} + \frac{1}{C_d} \tag{2.2}$$

Typical values of C_{sc} lie in the range 1-10 μFcm^{-2} (for moderately doped semiconductors) [70], C_H is of the order of 100 μFcm^{-2} for high electrolyte concentrations and C_d is of the order of 10 μFcm^{-2} for dilute solutions [71].

2.4.1 Measurement Procedure

The device schematic for the measurement of photo-capacitance is shown in Fig. 2.11. Following are the details of the methods and set up:

- The polymer solutions were made in chlorobenzene solvent and spin cast on the electrode-glass substrates inside the glove box. The substrates were annealed at 80^{o}C for 15 min.

- ITO coated glass was used as the bottom electrode.

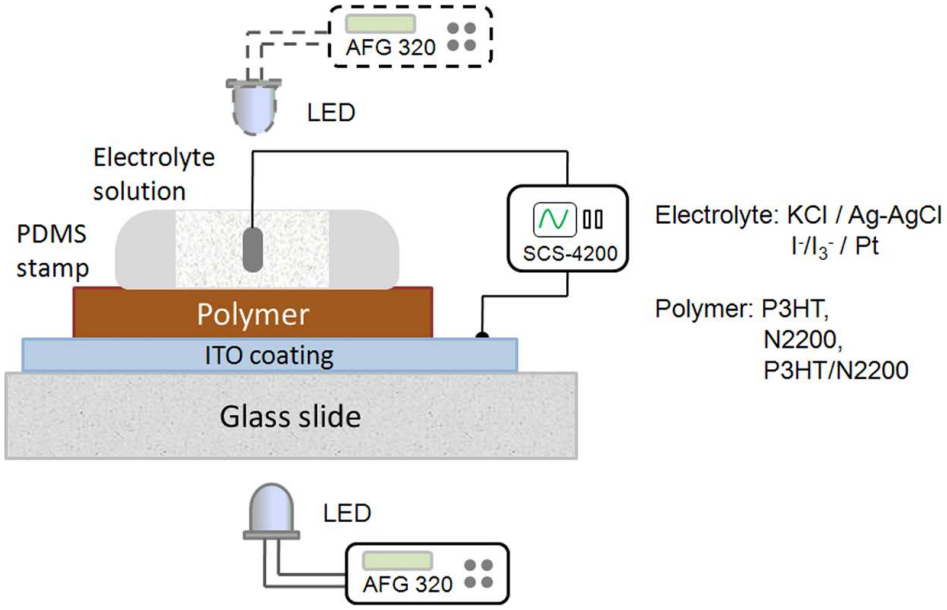

Figure 2.11: *Experimental set-up for measuring photo-capacitance.*

- Two kind of electrolytes were used : KCl solution (100 mM) and 3-propyl 1-methyl imidazolium iodide (referred here as PMII). The latter is a solvent free electrolyte and involves I^{3-}/I^{-} as the redox couple. PDMS wells were made to hold the electrolyte solution on top of the polymer films.

- Top electrode was Ag/AgCl pellet for KCl and Platinum coated FTO glass for PMII.

- White LEDs were used for illumination; the waveforms were controlled using a Function Generator (Sony Tektronics AFG320).

- Device illumination was from the polymer-electrode side.

- Parameter analyzer SCS4200 (Keithley Instruments) was used to measure the capacitance across the two device terminals. C_p-G_p mode was used in the KITE program. Before starting the measurements, confidence-check was done and R and C values of the contacts as well as connection wires were

also taken into account.

2.4.2 Photo-capacitance at various frequencies

The photocapacitance measurements were done with two type of devices :

ITO-(P3HT:N2200)Blend-KCl(100 mM)-Ag/AgCl and,

ITO-P3HT-PMII-Pt.

The parameter analyzer was connected across the ITO electrode and the Ag/AgCl or the Pt electrode. The frequency of measurement was initially set to 10 kHz (30 mV r.m.s) and the capacitance C of the device was measured as a function of time. In between one scan, the device was photo-illuminated for a period of 500 msec. The C-t scan with transient photo-illumination was then repeated for higher frequencies (up to 100 kHz).

Observations:

- Capacitance C is a function of frequency ω. C(ω) monotonically decreases with increasing ω (Fig. 2.12) both in dark as well as under illumination.
- At a fixed ω, when light falls on the device, the capacitance changes.
- This change in capacitance depends on ω.
- At low ω, $C_{Light} > C_{Dark}$. However, at high ω, $C_{Light} < C_{Dark}$. Figure 2.13(a) shows the observed results for the device with blend as the active polymer layer and Fig. 2.13(b) shows the results for the P3HT device.
- If $\Delta C = C_{Light} - C_{Dark}$, then $\Delta C > 0$ at low ω whereas $\Delta C < 0$ at high ω. We define $\Delta C/C_{Dark}$ as differential photo-capacitance.

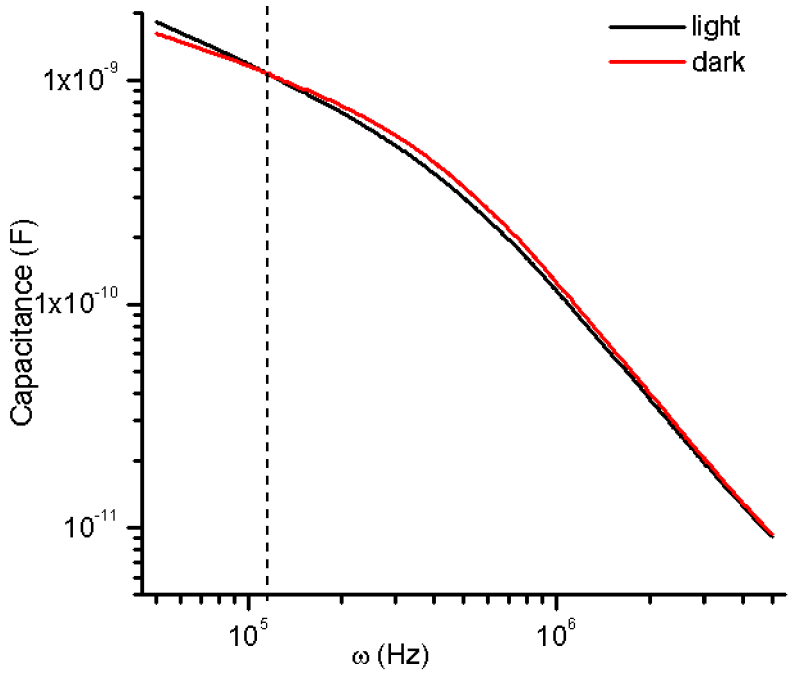

Figure 2.12: *Capacitance (in dark as well as under illumination) plotted as a function of frequency for P3HT:N2200 blend film with 100 mM KCl electrolyte. Similar trend was observed with P3HT as well. The critical frequency of cross-over can also be seen in this plot.*

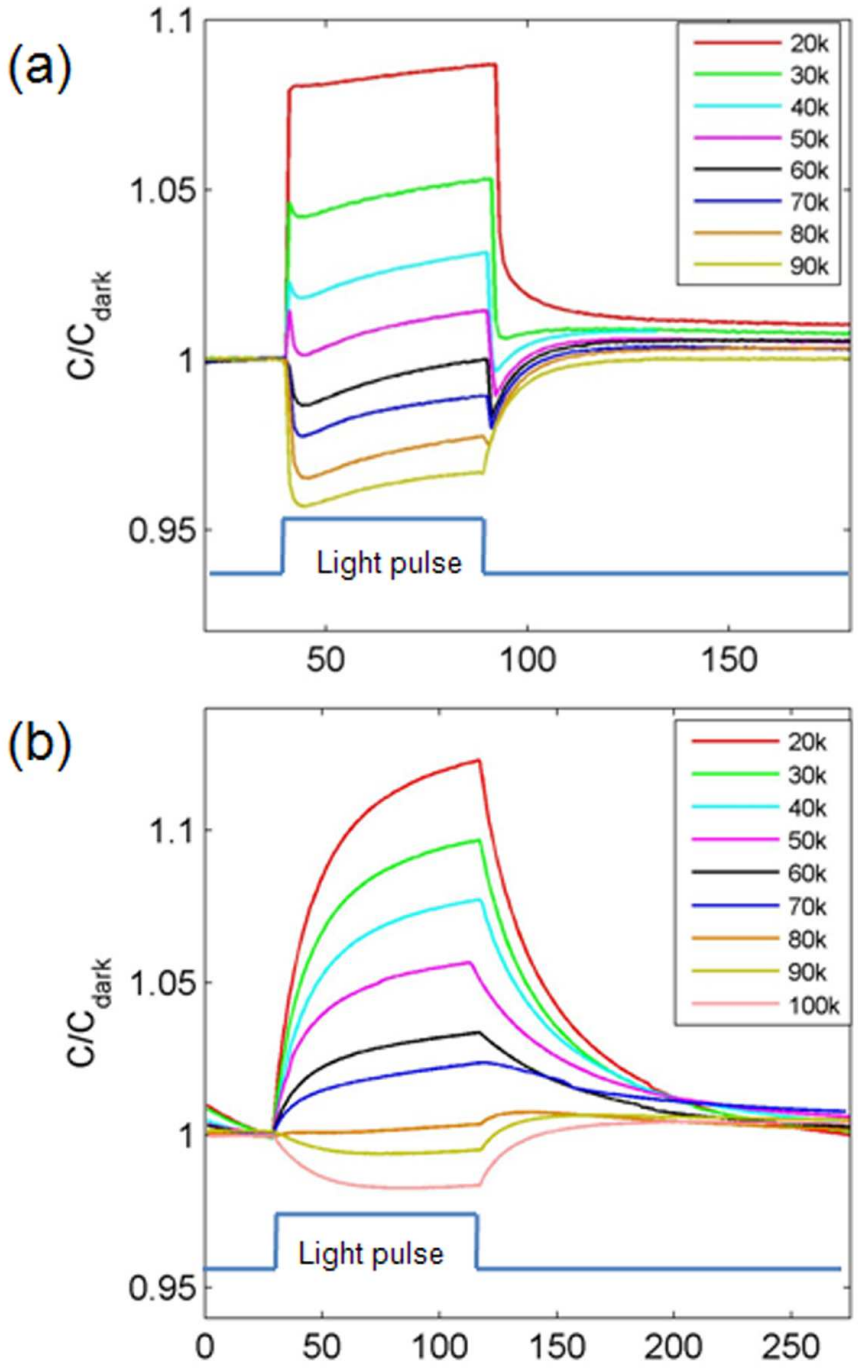

Figure 2.13: *Photo-capacitance as observed for (a) P3HT:N2200 Blend and (b) Only P3HT as active polymer layer in between ITO and 100 mM KCl. The duration of light pulse is 2.5 s.*

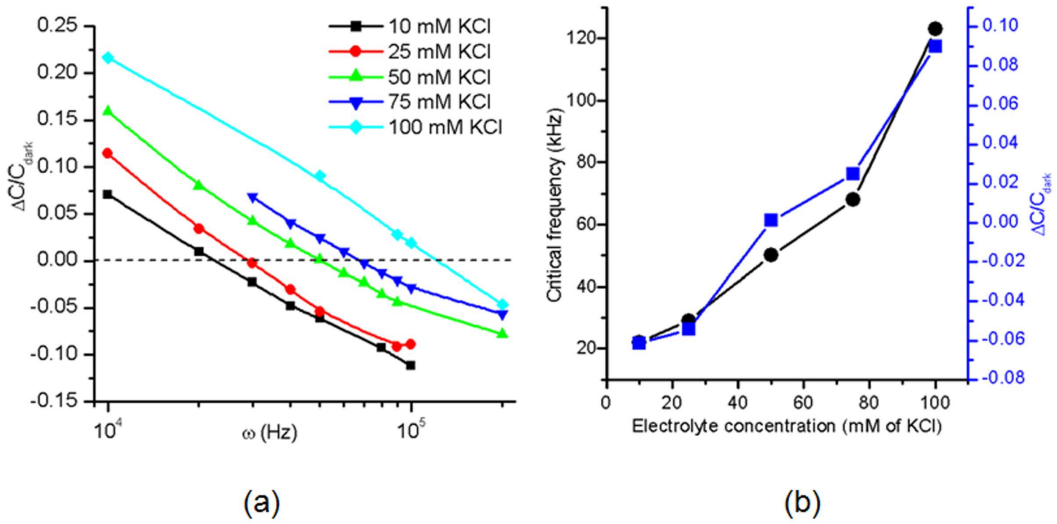

Figure 2.14: *(a) Differential photo-capacitance plotted as a function of frequency ω (b) Critical (cross-over) frequency and differential photo-capacitance as a function of electrolyte concentration.*

- There exists a critical (cross-over) frequency at which differential photo-capacitance changes its sign from positive to negative (Fig. 2.14).
- The cross-over frequency is higher for a higher concentration of electrolyte.
- The differential photo-capacitance, $\Delta C/C_{Dark}$ follows a similar trend as the critical frequency when plotted as a function of bias (Fig. 2.14(b)).
- The time constants of photo-capacitance from blend polymer system are less than 50 ms while for P3HT, time constants are of the order of 1 s.

2.4.3 Dependence of polymer-electrolyte capacitance on applied bias

The semiconductor analyzer system SCS4200 was used for the C-V measurements as well. The potential sweep was done from -2 V to +2 V with steps of 0.1 V and

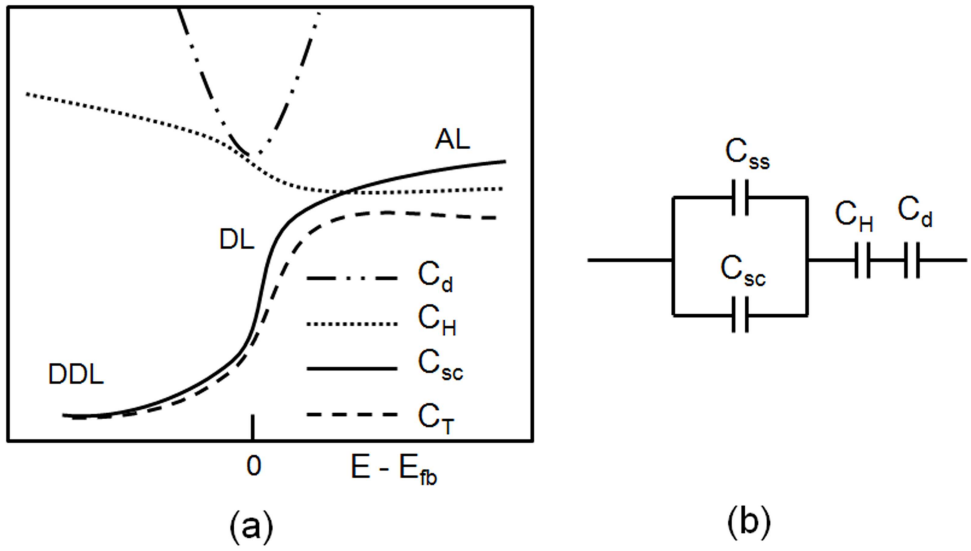

Figure 2.15: *Schematic of a C-V plot for a p-type semiconductor: C_{sc} is the space charge capacity of the semiconductor, C_H is the Helmholtz layer capacitance, C_d is the capacitance of the diffuse layer of charges in the electrolyte and C_T is the total capacitance. E_{fb} is the flat band potential of the semiconductor and E is the applied bias. AL, DL and DDL represent the accumulation, depletion and deep depletion regimes of the space charge capacitance respectively.*

hold time of 10 s at each bias point. The results shown are for ITO-P3HT-PMII-Pt device. We have plotted C vs. bias and C^{-2} vs. bias for both dark and under illumination with white light (Fig. 2.16).

The typical C-V behavior of C_{sc}, C_H and C_{dl} for a p-type semiconductor are shown as a schematic in Fig. 2.15. The diffuse layer capacitance C_d on the electrolyte side is almost dependent of the bias. The net capacitance resembles the profile of C_{sc}.

Observations

- C(V) is a function of ω.
- At low ω (around 10 kHz), the C-V curve follows the expected curve for a p-type semiconductor as shown in Fig. 2.15.

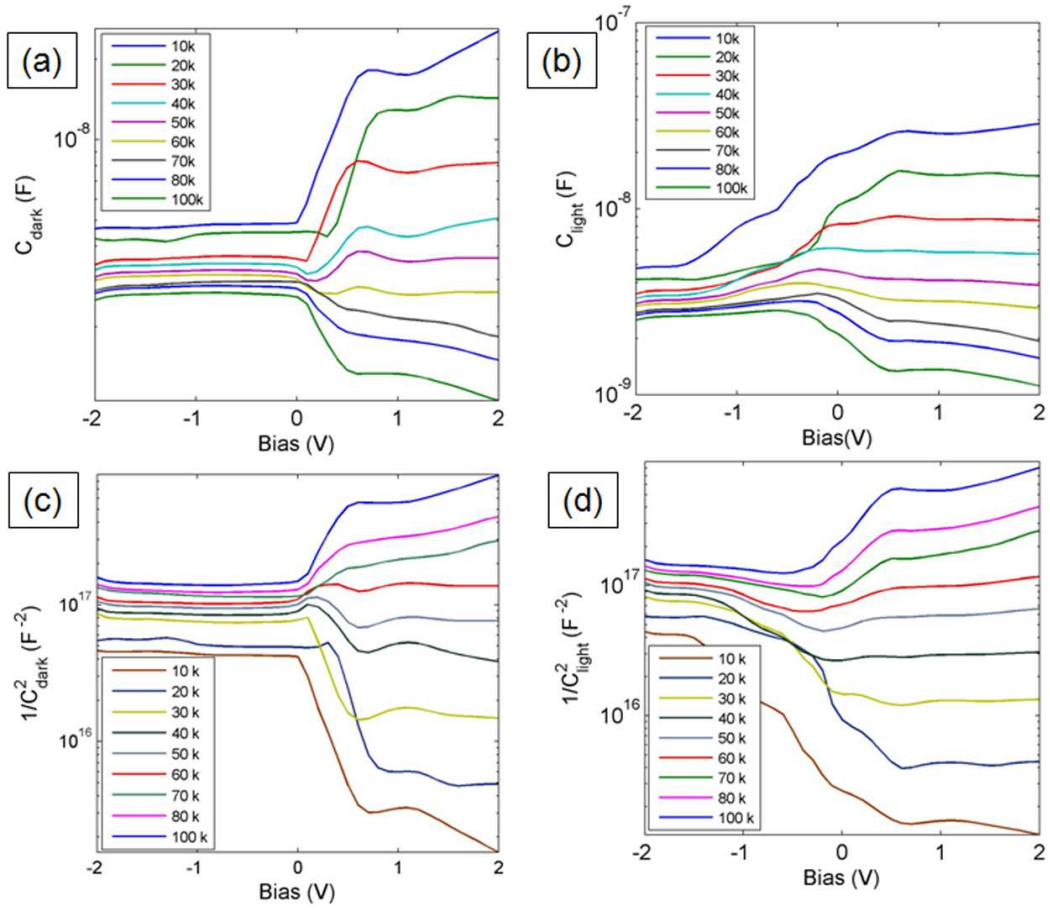

Figure 2.16: *C-V plots obtained at various frequencies ω for P3HT-PMII semiconductor-electrolyte system (a) In dark (b) Under constant white light illumination. Corresponding C^{-2} vs. applied bias plots are shown in (c) and (d).*

- At high ω (around 100 kHz), the C-V curve changes its slope in the positive bias region.
- There is a critical (cross-over) frequency at which this transition occurs.
- Under constant illumination, the C-V plots shifts to the right.
- Also plotted are C^{-2}-V plots and the same cross-over is observed.

2.4.4 The Origin of Cross-over Frequency

The ions in the electrolyte have a relatively lower mobility than the electrons and holes on the semiconductor side. The response to ions to an ac signal frequency ω is therefore slower. Owing to this reason, C_H has a steeper dependence on ω than C_{sc} [72, 73]. Therefore, at *low* ω's, the net C is dominated by C_{sc} but at *high* ω's, it is dominated by C_H.

Analysis of Results

The photo-generation of charge carriers in the polymer semiconductor film leads to a decrease in width of the space charge region, in turn leading to an increase in C_{sc}. At low ω therefore, the net capacitance increases and the differential photo-capacitance is positive. However, photo-illumination also generates a photo-potential at the interface such that a small field is produced in a direction opposite to the existing field across the semiconductor-electrolyte junction [70]. Hence, there is a decrease in the field across the Helmholtz layer which reduces the polarization of the adsorbed water molecules in this layer. This leads to a decrease in ϵ and hence, a decrease in C_H, as C_H is given by $C_H{=}\epsilon/d_H$. Therefore, at high ω, the

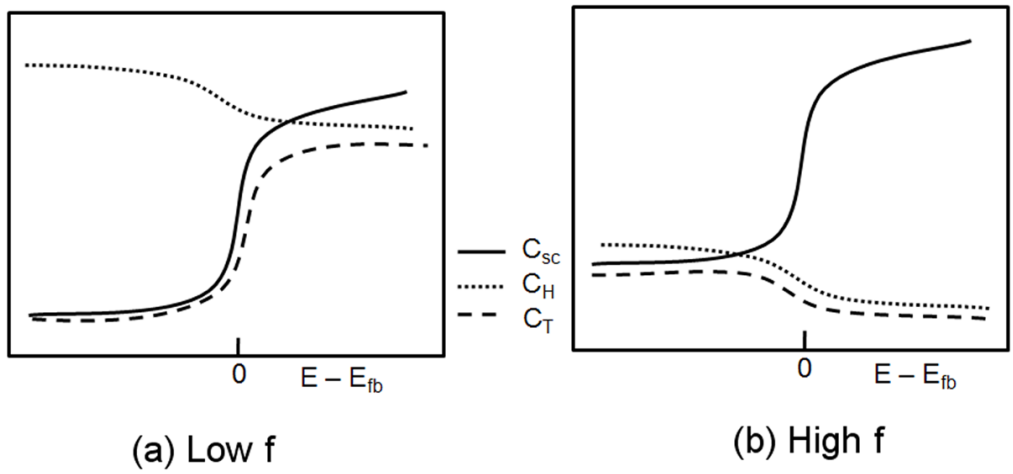

Figure 2.17: *Comparison of the C-V plot for a p-type semiconductor like P3HT : C_{sc} is the space charge capacity of the semiconductor, C_H is the Helmholtz layer capacitance, C_T is the total capacitance, E_{fb} is the flat band potential of the semiconductor and E is the applied bias. (a) At low ω, C_T is similar to the profile of C_{sc}; (b) At much higher ω, C_T follows C_H.*

net capacitance under illumination is lower than that in dark and differential capacitance is negative.

In the C-V plots, the total capacitance follow the C_{sc} profile at low frequencies. At high frequencies however, it is dominated by C_H and hence its slope changes. This is shown in the schematic in Fig. 2.17

2.5 Summary

The transient photo-response of a metal - organic semiconductor - electrolyte device is dominated by the interface of the polymer on the two sides. Photo-voltage from a thick film was compared to the thin film of the polymer. The intensity and wavelength dependence of rate of charge generation (and therefore photo-voltage) in these devices could also be observed.

A consistent set of observations was also obtained for the capacitance measured over a period of time (C(t)) and as a function of bias (C(V)) in dark and under illumination at different frequencies. The cross-over frequency was observed to be a characteristic feature of the polymer-electrolyte interface.

The presence of fundamentally different processes in each medium leads to interesting features in the photovoltage and photocapacitance measurements. The features originate from the photophysical processes in semiconductor organics and the charge dynamics in the electrolyte medium. We have attempted to understand the results based on these bulk and interfacial events. Moreover, the method of frequency sweep can be useful to probe the role of individual material layers of a hybrid device.

CHAPTER 3

INTRODUCTION TO THE ELECTRICAL PROCESSES IN NEURONS AND RECORDING TECHNIQUES

The work described in the next chapter of the thesis involves electrical signal recording from a nervous tissue using extracellular Micro-Electrode Array (MEA) system. This chapter gives a brief overview of the basic theory behind the neural processes and typical extracellular recording methods that will be used in next chapter. A detailed description of these topics can be found in a large number of comprehensive reviews and text books (for eg. the book 'Principles of Neural Science and Behavior' by E.R. Kandel) available in literature. The brief topics listed below are limited to the basic concepts required to understand the methods and results of the next chapter.

3.1 Signal transport in the nervous system

Brain and other components of the nervous system communicate via electrical and chemical wiring networks. The nervous system integrates countless bits of information and generates appropriate reactions by sending electrochemical impulses through nerve cells to effector organs such as muscles and glands. The nerve cells or neurons act like the signal transmitting electric wires.

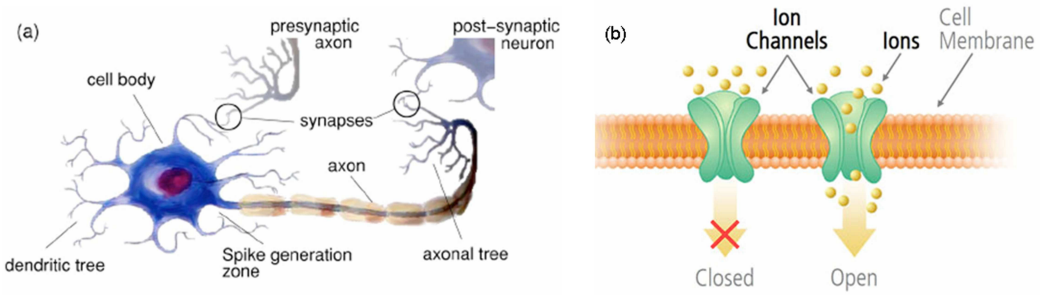

Figure 3.1: *A typical Nerve Cell. (a)Basic Structure (b)Ion channels span the entire membrane and determine the changes in membrane potential. Adapted from [74].*

The basic structure of Neurons

Nerve cells or neurons are the basic unit of the central nervous system and are supported by another type of cells called glia. There are more than 10^{11} neurons in the human brain. Though different in structure and function, all neurons share the basic architecture (Fig. 3.1). The dendrites receive signals from other neurons; the cell body contains the DNA encoding neuronal proteins and the complex apparatus for synthesizing them; the axon projects over long distances to target cells (for example, other neurons or muscle cells); and the nerve terminals release neurotransmitters at synapses with targets.

3.1.1 Characteristics of Neuronal Signals

Signaling in the nervous system depends on the ability of nerve cells to respond to small stimuli like sounds, light, smell etc. The response of a neuron is a rapid change in its membrane potential, i.e. potential difference across the cell membrane.

The rapid changes in the membrane potential are mediated by various types of *ion channels*. Ion channels are a class of proteins that span the plasma membrane of all nerve and muscle cells. They regulate the flow of ions across the plasma

membrane of these cells. Ion channels are heterogeneous, i.e. each type of channel is selective to only one type of ion like only K^+ or Na^+. Apart from ion *selectivity*, they also differ in the mechanism of *gating*.

3.1.2 The equivalent circuit of a membrane

The equivalent circuit of plasma membrane includes voltage sources, conductors, a capacitor, and a current generator. The lipid bilayer structure of the plasma membrane separates two conducting solutions of ions: the cytoplasm and the extracellular fluid and therefore acts like a capacitor. However, the presence of ion channels provides a conductive path to certain ions. The circuit is shown in Fig. 3.2.

When the cell is at rest, there exists a balanced passive ionic flux into and out of the cell so that the charge separation across the membrane remains constant. The value of the resting membrane potential in nerve cells is determined primarily by resting channels selective for K^+, Cl^-, and Na^+. The concentration gradient of an ion determines the value of the battery corresponding to it and the permeability of plasma membrane to certain ion determines the conductance values.

The value of the rest potential is given by the Goldman's equation:

$$V_m = \frac{(E_{Na} X g_{Na}) + (E_K X g_K) + (E_{Cl} X g_{Cl})}{(g_{Na} + g_K + g_{Cl})} \tag{3.1}$$

Here, the values of the E's are calculated from the Nernst Potential of the corresponding ion, for eg.

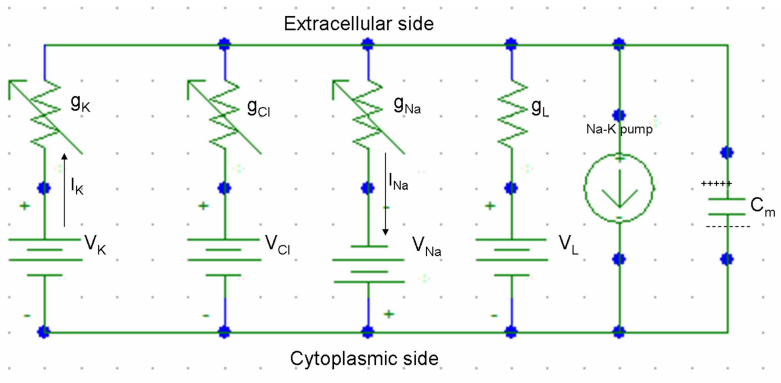

Figure 3.2: *Equivalent circuit of a plasma membrane of a typical neuron, as shown in [75].*

$$E_{Na} = \frac{RT}{F} \ln \frac{[Na^+]_o}{[Na^+]_i} \tag{3.2}$$

At rest, the potential across a typical neural membrane ranges between -60 mV to -80 mV.

During signaling the changes in membrane potential (action potentials, synaptic potentials, and receptor potentials) are caused by substantial changes in the membrane's relative permeabilities to these three ions in turn leading to changes in the net charge separation across the membrane.

3.1.3 The Action Potential

An action potential is a regenerative electrical signal whose amplitude does not attenuate as it moves down the neuronal axon. It arises from sequential changes in the membrane's selective permeability to Na^+ and K^+ ions. The membrane's passive properties influence the speed at which action potentials are conducted.

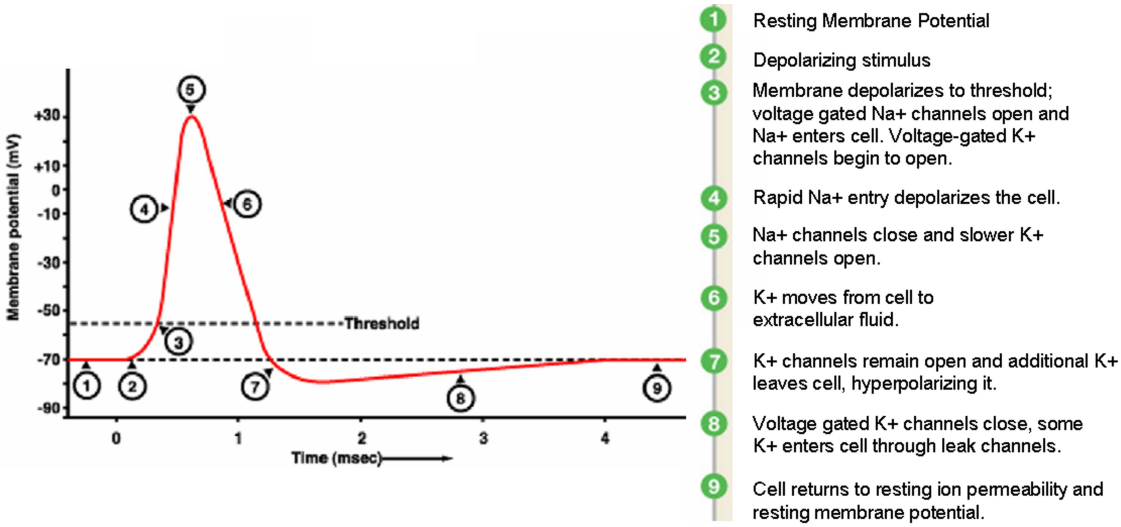

Figure 3.3: *Schematic of a typical Action Potential (spike) and the sequence of events involved.*

The action potential is generated by the flow of ions through voltage-gated Na^+ and K^+ channels. On stimulus, the membrane becomes more permeable to Na^+ and an inward Na^+ current flows causing the membrane get depolarized upto +40 mV. After a certain level of depolarization, the voltage gated K^+ gates open and lead to a net outflux of K^+ to balance the charge. This causes the fall in the action potential. The region of hyperpolarization appears due to more K^+ outflux than Na^+ influx. At this instance, the Na-K pump gets activated and it drives the respective concentrations of the two ions to their initial state until the cell is at its rest potential. The cell is inactivated during this period. The sequence of events is shown in Fig. 3.3.

Action potentials arise only if the depolarizing stimulus crosses certain threshold and hence, it is an all-or-none phenomenon. Also, the typical spike width in the nervous system are about $1-5$ ms.

3.2 Typical Methods in Electrophysiology

Recording electrical signals from excitable cells

Electrophysiology is considered to have begun in the late 18th century when Luigi Galvani noted that application of an electrical pulse to a frog's nerve evoked a twitch in the leg muscle. After such of studies on bioelectricity, the first successful measurements of resting and action potentials came about from the studies on giant squid axon by Hodgkin and Huxley in 1939. Further, the development of voltage clamp technique by Cole in 1949 [76] led Hodgkin and Huxley to deduce the key roles played by Na^+ and K^+ ions in the action potentials; this work was together published in 1952 [77–80].

A revolution in understanding the mechanism of ion flow across the cell membranes in excitable cells like neurons was the development of patch clamp technique by Neher and Sakmann in 1976 [81]. The patch-clamp technique has made it possible to record the current flow through single open channels.

Hodgkin and Huxley were awarded the Nobel Prize in physiology in 1963 while Neher and Sakmann received the same in 1991.

3.2.1 The Hodgkin-Huxley Equations

The experiments done on the giant squid axon by Hodgkin and Huxley were based on voltage and clamp technique. In the voltage clamp method, the cell membrane is maintained at a known potential using a feedback circuit and currents across the membrane are recorded (Fig. 3.4(a)).

Based on the equivalent circuit model of the plasma membrane and their experimental observations, they developed a model of an excitatory neuron. This model consists of the equation for the total membrane current, I_m, given by [80]:

$$I_m = C_m \frac{dV}{dt} + I_K + I_{Na} + I_L \tag{3.3}$$

or,

$$I_m = C_m \frac{dV}{dt} + g_K(V - E_K) + g_{Na}(V - E_{Na}) + g_L(V - E_L) \tag{3.4}$$

Further, the conductance values were modeled as:

$$g_{Na}(V,t) = g^0_{Na} m^3(V,t) h(V,t); g_K(V,t) = g^0_K n^4(V,t) \tag{3.5}$$

Here, L represents the leaky membrane currents and C_m is the membrane capacitance.

The solution very well fitted all the current profiles based on the activation (m,n) and inactivation(h) parameters of the voltage gated ion channels. Since this model is not relevant for the work described in the next chapter, it is not described in further detail.

3.2.2 Patch Clamp and Multi-Electrode Arrays

The Patch Clamp Technique

To monitor the activity of single ion channels or an entire nerve cell, the most common practice in physiology labs is the patch clamp. Patch clamp technique is a refinement of the voltage clamp. The recording uses a single glass micropipette (tip diameter close to one micron) as an electrode. This electrode can be sealed on

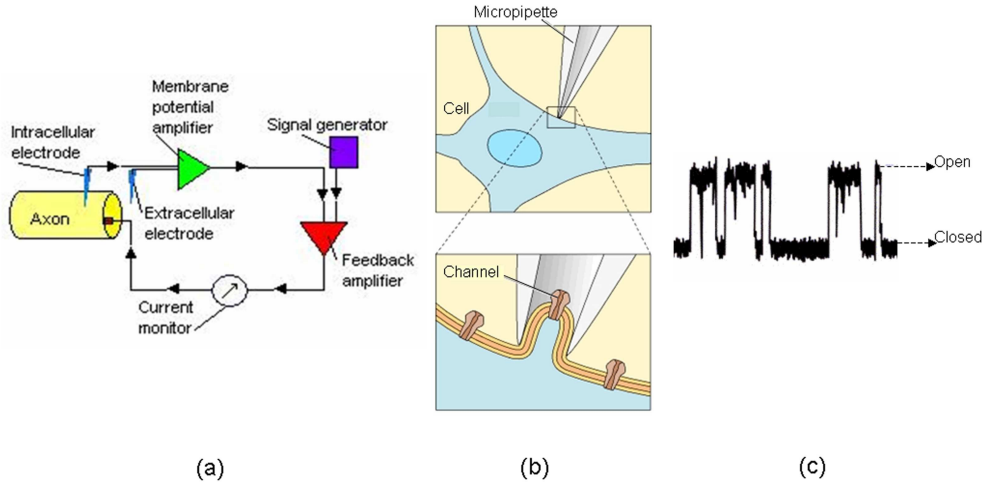

Figure 3.4: *The Patch Clamp (a)Schematics of the voltage clamp technique. (b)The patch micropipette and gigaohm seal across a channel. (c)Typical single channel current recordings: current drops to baseline when the channel gets closed in response to a stimulus or vice versa. Adapted from [82].*

to the signalling cell.

The interior of the pipette is filled with a solution matching the ionic composition of the bath solution, as in the case of cell-attached mode, or the cytoplasm for whole-cell recording mode. A chlorided silver wire is placed in contact with this solution and conducts electrical current to the amplifier.

The micropipette is pressed against a cell membrane and suction is applied to assist in the formation of a high resistance seal between the glass and the cell membrane (a "gigohm seal" or "gigaseal"). The high resistance of this seal makes it possible to electronically isolate the currents measured across the membrane patch with little competing noise, as well as providing some mechanical stability to the recording. Figure 3.4(b) schematically describes this technique.

Patch clamp can be operated in both voltage and current clamp recording modes. The current clamp technique records the membrane potential by injecting current into a cell through the recording electrode. In current clamp mode the membrane

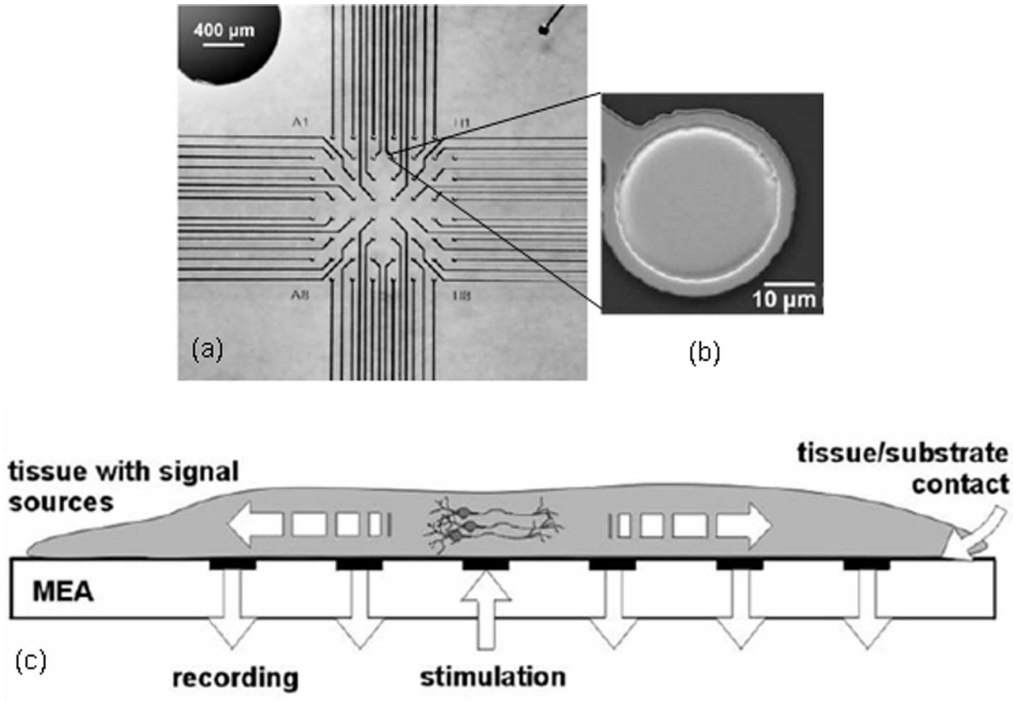

Figure 3.5: *Multi-Electrode Array.(a) A standard planer 8X8 MEA with 60 electrodes. (b)Single electrode: size can vary from 10µm to more than 200µm depending on application. (c) MEA recordings are extracellular; can be used to stimulate and simultaneously record from an entire tissue, thereby providing spatial information. Adapted from [83].*

potential is free to vary, and the amplifier records whatever voltage the cell generates on its own or as a result of stimulation. Figure 3.4(c) shows typical patch clamp current recording from a single ion channel.

The MEA Technique

Instead of the patch clamp, we have used a different approach to monitor the electrical signals from the retinal neurons. Briefly, recording the cell potentials *extracellularly* using a Micro-Electrode Array (MEA) is done by a set of 60 or more planar metal electrodes on a glass chip, each electrode connected to a voltage and filter amplifier. This is a *field recording* where the local changes in ion currents in

the extracellular fluid are monitored around the signalling cell or a group of cells. MEA technique was first introduced in 1972 by Thomas et. al [84] with an aim of drug screening and discovery in cardiac and neural research.

MEAs score over the patch clamp technique in cases where both temporal as well as spatial resolution is required. It provides the ability to record from several sites in parallel. Also, changes in the electrical activity can be monitored for long periods of time that can not be achieved through conventional glass or tungsten microelectrodes. Figure 3.5 shows a standard 8X8 MEA and the basic principles of recording.

Since the MEA recording is extracellular, the signal to noise ratio depends on the distance between the source cell and the underneath electrode. Also, the difference in coupling mechanism between the membrane and electrode in a patch recording and an MEA recording usually leads to a difference in the amplitude and shape of signals recorded from the two techniques [83].

The utility of MEA technique can be demonstrated for many interesting problems. In the next chapter, the use of MEAs to record signals from a retinal tissue has been discussed. Because it will be dealt with in the next chapter, it is useful to list the salient features and visual processes involved in the retina. The following section includes a brief description of the structure and photo-induced processes within the retina.

3.3 Introduction to the Retina

Retina is the photosensitive sensory organ in the eye. It is a transparent layer of cells, consisting of a complex network of neurons. It encodes the spatiotemporal light signals into neural (or electrical) signals and then transmits these signals

through the optic nerve to the higher processing units of the brain for perception. Retina is considered to be the most easily accessible part of the central nervous system.

3.3.1 Structure of the Retina

In advanced eyes like those of the mammals (mice, rabbits, cats, monkeys and other commonly studied species), the visual image is focused onto the retina by the optical components of the eye that include the lens and the cornea located at the eye's anterior portion.

The retina is attached to the interior walls of the eye at the Ora Serrata. Just behind the retina is a layer of pigment epithelium that nourishes the retinal photoreceptors. In most animals, the pigment epithelium cells contain black pigment melanin that absorbs any excess light not captured by the retina and prevents it from getting reflected back to retina (which would otherwise degrade the visual image). Between the pigment epithelium and the sclera (opaque outermost layer at the back of the eye) is a layer of vascular tissues called the choroid. This layer provides oxygen and nourishment to the retinal layers. Fig. 3.6 shows the arrangement of these structures in a human eye.

The synaptic organization of retina is similar to other central neural structures, but it is comparatively simpler. Retina has a layered anatomical arrangement with five major classes of neurons linked in an intricate pattern of connections. The identification and classification of the retinal neurons began more than 100 years ago by S. Ramon y Cajal.

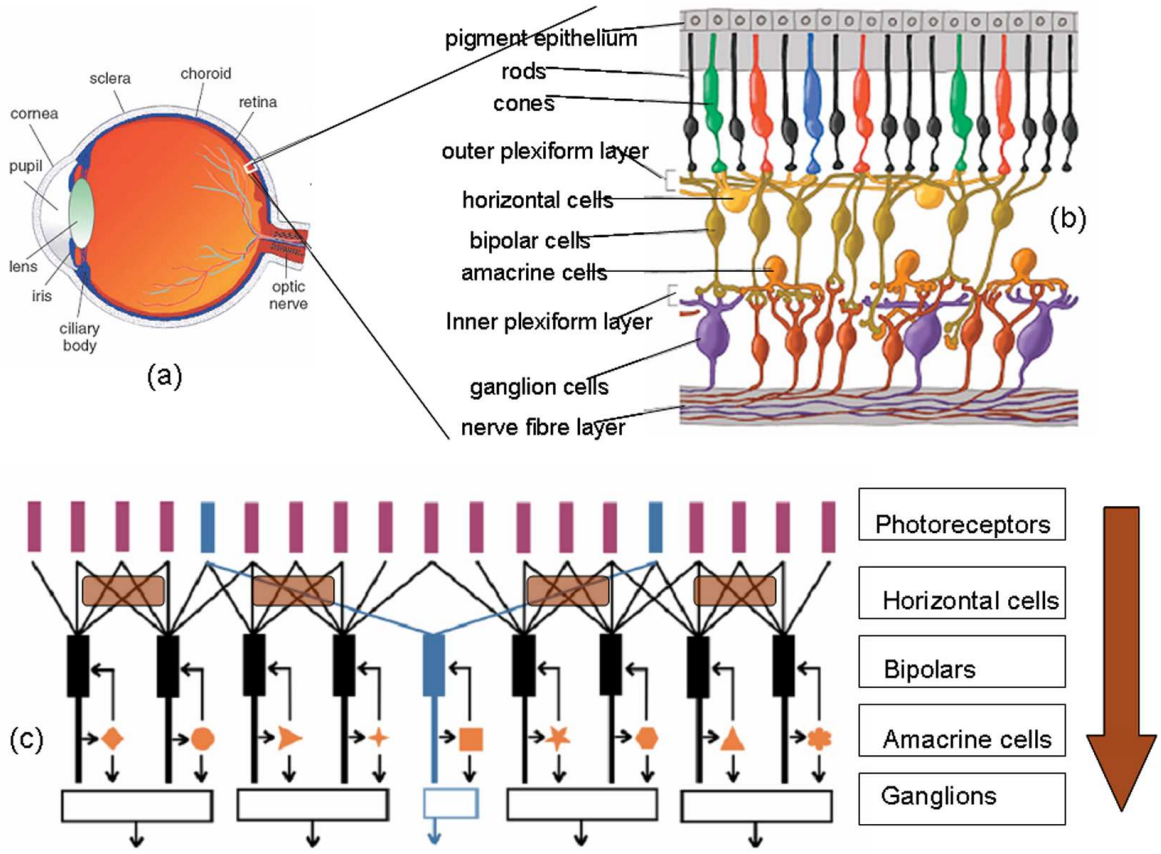

Figure 3.6: *(a), (b) Basic structure of Eye and the layered arrangement of the retinal neurons. Adapted from [85]. (c) Block diagram of the various connections that exist in between the neuronal layers. The block arrow shows the direction of signal transduction.*

(a) The photo-receptors: Rods and Cones

Input elements

The photoreceptors form the outermost layer of the retina. Both rods and cones have similar morphology. They consist of inner and outer segments and synaptic terminals. While the inner segments control the metabolism of these cells, the outer segments have the membranous disks that have the light absorbing photo pigments. The synaptic terminals make contact with the photoreceptor target cells. Figure 3.7 shows the morphology of these receptors. Following are the main features:

- The sensitivity of rods to the incident photons is many times greater than the cones. A single photon can elicit an electrical response in rods, but cones would typically require hundreds of those photons to respond.
- Rods amplify signals more than the cones. It is due to this reason that rods are responsible for night vision while cones mediate the day and color vision.
- Cones are faster in response than rods. The integration times of cones are around 20 ms while for rods its around 100 ms. This means that cones can detect a flicker of atleast 50 Hz, but rods can not detect flickers of frequency greater than 10-12 Hz.
- Rods outnumber cones roughly by a ratio 20:1. Cones are centered in the fovea where the visual image is least distorted.
- Many rods converge onto the same bipolar cells - the difference in their response is averaged out. Hence, cones being less in number still provide a better temporal as well as spatial resolution than rods.

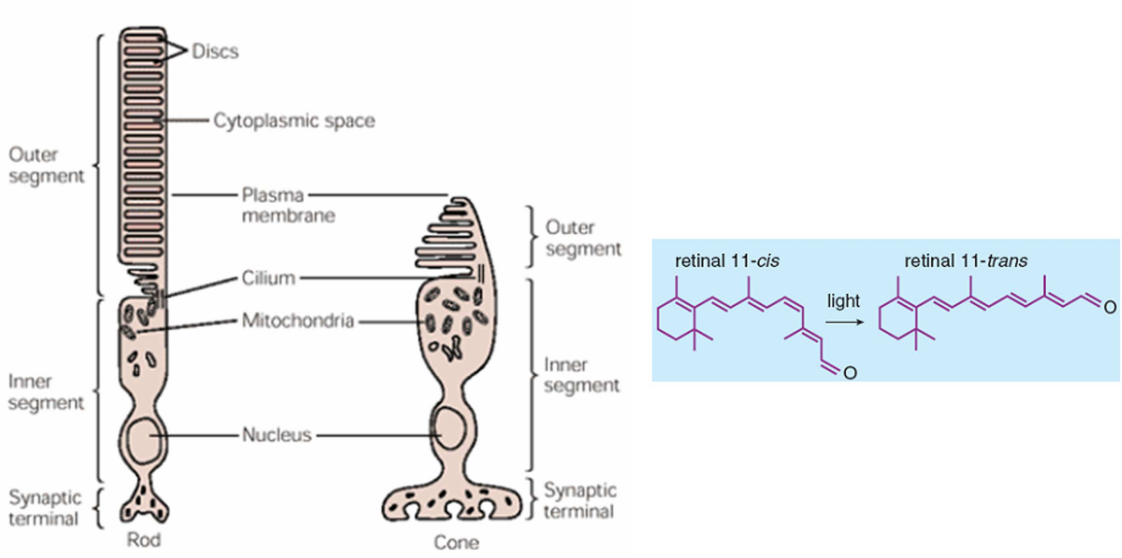

Figure 3.7: *Morphology of the photoreceptors. (a) Rod and cone cells. (b)Incident light causes cis- to trans- retinal conformation change in the rhodopsin; this is the starting point of signal transduction in the retina. Adapted from [75].*

- Most mammals have a single type of rods (peak sensitivity 500 nm) but two types of cones: M-type or green (peak sensitivity 550 nm) and S-type or blue (peak sensitivity 450 nm). Primates like humans and monkeys however are tri-chromatic, i.e. they have additional L-type or red cones which have sensitivity for longer wavelengths. The types correspond to the sensitivity of the visual pigments contained inside their outer segments.
- The output electrical response of photoreceptors to a light stimulus is a graded change in membrane potential (instead of a spike).

(b) Bipolar and AII cells

Forward transmission elements

The dendrites of the bipolar cells collect synapses from photoreceptors. The rod bipolar cells connect only to rods and the cone bipolar cells connect only to cones. Bipolar cells are of two types: ON and OFF, i.e. some of the bipolar

cells are exited by light onset while some are exited by light offset.

(c) Horizontal and Amacrine cells

Lateral transmission elements

While horizonatal cells mediate signals from rods and cones into bipolar cells, amacrine cells are of various types and mediate signal connection patterns between the receptors and bipolars as well as bipolars and the ganglions.

(d) Ganglion cells

Output elements

Ganglion cell bodies form the innermost cellular layer of the retina. Their dendrites penetrate the inner plexiform layer to collect excitatory synapses from bipolar axons and both excitatory and inhibitory synapses from amacrine cells. Ganglion cell axons enter the optic nerve and extend to the brain.

Unlike the photoreceptors, the ganglion cells transmit information as a train of **action potentials**. The response of the ganglion cells depends critically on the precise spatial and temporal patterns of light that stimulate the retina. This is controlled by the three types of interneurons described above.

Similar to the bipolar cells, ganglion cells are also of ON and OFF types. Ganglion cells are specialized for detection of contrast and rapid changes in the visual image. This is accomplished by their center-surround receptive field of organization.

3.3.2 Signal Transduction in the Retina

Stimulation by light results in a complex signalling by neurons within the various layers of the retina. There exists a three stage cascade of biochemical events in the

photoreceptor cells of the retina which results in photo-transduction.
The key molecule in this process is the nucleotide cyclic guanosine 3-5 monophosphate (cGMP). Cyclic GMP controls ionic fluxes by opening a specialized species of ion channels, the cGMP-gated ion channels, which allow an inward current carried largely by Na^+ ions to flow into the cell. In dark, the concentration of this molecule is in excess. Thus, the cGMP gated ion channels are in open state and there exists a constant inward Na^+ current. Hence, in dark, cells are in the depolarized state. Following steps briefly describe the signal cascade [75]:

Step 1: Light is absorbed by the visual pigment *Rhodopsin* in the outer segment disks of rods and cones. Rhodopsin consists of a protein *opsin* and a chromophore *retinal*. When non-activated, retinal exists in an 11-cis isomeric form and fits inside the binding site of opsin. However absorption of light causes the retinal to change from 11-cis to all-trans conformation. This retinal form no longer fits into the opsin binding site and is transported from photoreceptors to the pigment epithilial cells for replenishment by trans-retinol.

Step 2: The activation of rhodopsin in presence of light causes the activation of enzyme phosphodiesterase which hydrolyses the cGMP molecules and in turn causes the cytoplasmic concentration of cGMP to reduce.

Step 3: The light evoked decrease in cGMP causes the cGMP gated ion channels to close. This leads to the hyperpolarisation of the photoreceptors.

Figure 3.8 briefly shows the sequence of events described above.

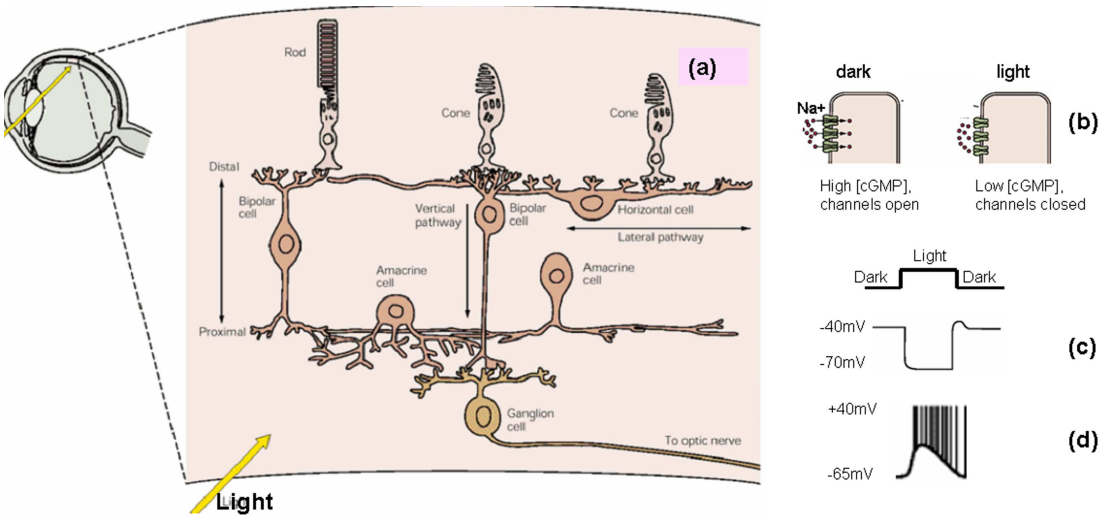

Figure 3.8: *Signal Transduction in the retina. (a) various signal pathways across the layers (b) cGMP ion channels close in presence of light thereby hyperpolarizing the photoreceptors (c); (d) corresponding spike trains produced on an ON-center ganglion cell. Adapted from [75].*

The changes in membrane potential of the photoreceptors are transduced as electrical signals through their synapses to the interneurons and then to the ganglions. It is in the ganglion cells that these signals are encoded into action potentials (spikes) corresponding to the image and then transferred to brain for higher processing.

The above topics provide the basic understanding of the output signal profiles from the retina. The following chapter describes the application of MEAs to record such electrical signals from a retinal tissue. These signals recorded from standard MEAs are then compared to the signals from a conducting-polymer modified MEA. The advantages of using a conducting polymer MEA over the standard MEAs are then discussed.

CHAPTER 4

CONDUCTING POLYMER COATED MEAS FOR SIGNAL RECORDING FROM THE RETINA AND NOISE ANALYSIS

4.1 Motivation

Micro-electrode arrays (MEA) are widely used for signal recording and stimulation from cultured neurons or whole tissue mounts like hippocampus and retina. However, reducing the electrode size to microscale for higher spatial sensitivity increases the electrode impedance thereby leading to a lower sensitivity. Moreover, the recording with MEA is extracellular. Hence, the signal strength depends directly on the electrode-cell distance, i.e. the mechanical contact of tissues onto the MEA [83]. Various coatings such as lysin, laminin and nitrocellulose are used for better adhesion of tissues and cells on the MEAs [86]. However, these coatings are non-conducting and hence introduce an additional impedance factor.

The use of carbon nanotubes and silcon nanowires as neural interfaces has already been reported [87, 88]. Conducting polymers such as poly(-pyrrole) (Ppy) and poly-(3,4-ethylenedioxythiophene) (PEDOT) have also been considered as bioelectronic interfaces [89]. They have been used as scaffolds to grow neurons and are shown to be biocompatible [90,91]. It is also observed that conducting polymer layers enhance charge injection capabilities of underlying metal electrode sites [92] as well as improve the adhesion and attachment between neurons and electrodes [93].

PEDOT nanotubes were recently used for neural recordings and were shown to enhance quality of recording signals [94].

This chapter summarizes the observations and data analysis of signals recorded from retina whole mounts using MEAs modified with the conducting polymer PEDOT:PSS. It includes the comparison of these signals to those obtained with standard ITO and TiN MEAs.

4.2 Materials and Methods

4.2.1 Visual Stimulus

The visual stimulus is a 0.5 Hz diffuse full-field temporal square wave, 1 s light ON followed by 1 s light OFF, projected onto the in-vitro retina. White LED is used as the source and was controlled by a function generator (Sony Tektronix AFG320).

4.2.2 The MEA system

MEA holder and the voltage amplifier from Multichannel Systems (MCS), Germany were used and are shown in Fig. 4.1. The MEA grid is located at the center of a glass substrate and surrounded by a chamber to hold the perfusion fluid (about 0.5 ml). MEAs used were ITO MEAs from Ayanda Biosystems, Switzerland and TiN hexa-MEA from MCS. The disc microelectrodes of the ITO MEAs are made of transparent ITO with 60 microelectrodes in an 8x8 matrix arrangement with no electrodes at the four corners. Each microelectrode is a 40 μm diameter disc. The center-to-center distance between microelectrodes of this MEA grid is 200 μm. The TiN array is an hexagonal arrangement of the TiN microelectrodes with electrode

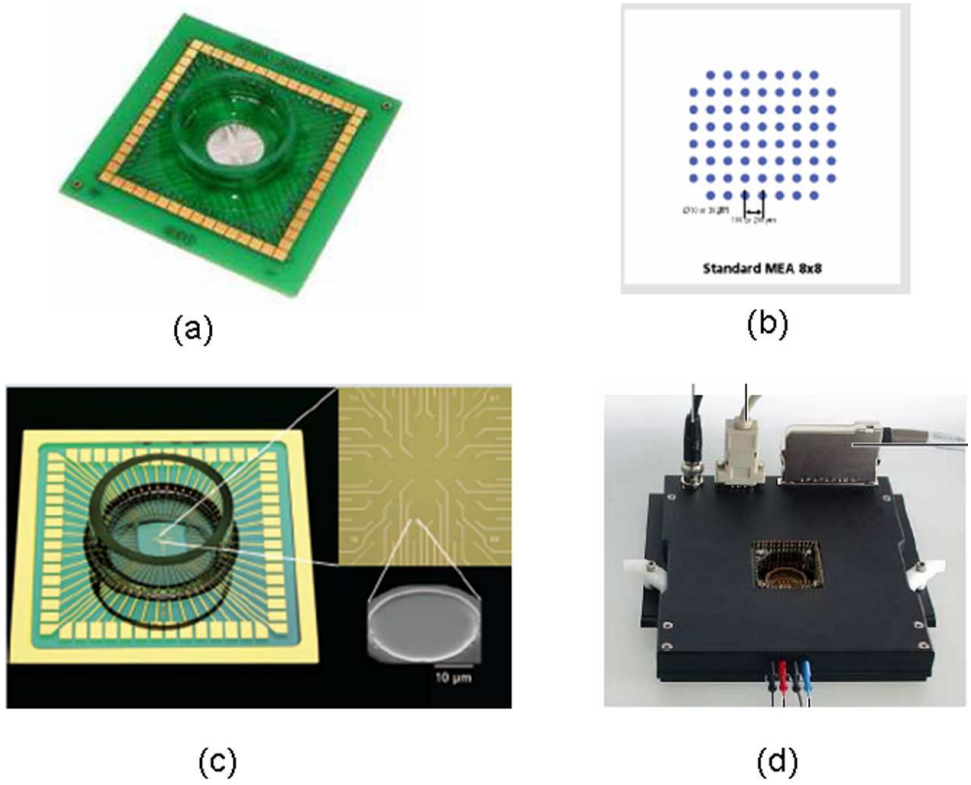

Figure 4.1: *(a)Standard MEA chip from Ayanda Biosys Corp. (b) 8X8 layout of the 60 electrodes. (c) 10µm diameter electrodes in a TiN array from MCS (Germany). (d) The MEA holder box which also contains the voltage amplifier. The MEA is placed inside this holder and spring contacts are made using 60 golden pins.*

diameter 10, 20, 30 μm and inter-electrode spacing 30, 60 and 90 μm respectively.

The electrodes are connected to the contact pads through tracks. The micro-electrodes and contact pads are exposed and the tracks are insulated with Silicon Nitride.

Reference Electrode

The reference electrode for the recording microelectrodes is a silver/silver chloride (Ag/AgCl) palette attached with a wire. The electrode palette is dipped into the Ames' medium solution (explained later in text) in the MEA chamber and its wire is attached to the ground terminal of the voltage amplifier.

MEA Cleaning, Storage and Usage

MEAs are cleared of any particulate debris deposited during storage in a glass case or retinal tissue debris deposited from a previous experiment. The cleaning procedure consists of two steps, ultrasonication at 10 kHz for 3 min followed rinsing with methanol. The MEA grid is observed under a microscope after cleaning to confirm effectiveness of the cleaning procedure. MEA is then stored in a 70 % ethanol/water solution after cleaning. It is rinsed with distilled water and then dried just before mounting the tissue on it. The lower surface of the MEA glass is usually marked with a tape underneath the MEA grid so that it is visible.

MEA Holder and Voltage Amplifier

The MEA holder and the voltage amplifier constitute a single unit, model number MEA- 1060-BC by MCS. The voltage amplifier is removable from the MEA holder. The voltage amplifier receives its power input from the DAQ PC. It has a gain of 1100 and a hardware bandpass filter with cutoff frequencies in the range of 1-5000 Hz. The voltage amplifier attaches to the microelectrodes of the MEA through 60 spring loaded pins. After placing the MEA in its holder, the voltage amplifier is placed vertically on top, pressed down and locked into place with clamps. The pins thus make electrical contact with the contact pads of the MEA. These pins connect to the voltage amplifier through toggle switches. The toggle switch allows one to ground a microelectrode if necessary. A microelectrode channel picking up excessive noise during an experiment is grounded, since its noise spreads to neighboring channels and decreases their signal to noise ratio. High noise appears on a channel if the respective contact pad of the MEA is not clean.

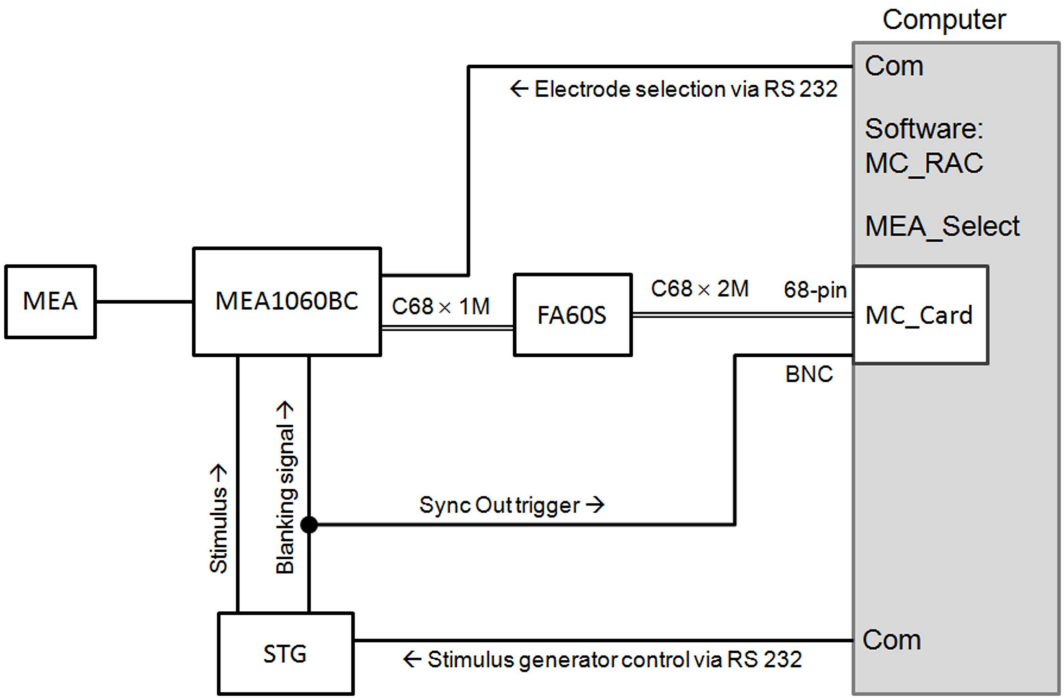

Figure 4.2: *Block diagram showing the hardware and software connections of the MEA system.*

4.2.3 The data acquisition system

Data acquisition PC is an Intel core-2 Duo equipped with a *16 channel* data acquisition board MC-Card (ME-System from MCS). The MC-Card accepts a connector from the voltage amplifier, which carries power signals to the voltage amplifier and 60 analog voltage channels from the voltage amplifier. In addition, it also accepts six BNC connectors for three analog inputs named A1, A2 and A3, and three digital inputs named D0, D1 and D2. The input voltage range is -4.96 V to +4.96 V for all analog channels and TTL levels 0 V and +5 V for digital inputs.

The schematic of electrical connections to the MC-Card are shown in Fig. 4.2. One BNC digital input was used to acquire the stimulus trigger signals from the function generator (Sony Tektronix AFG320).

The operating software used for MC-Card data acquisition is MC-Rack Version

3.9.0 by MCS. The MC-Card, configurable through MC Rack is capable of digitization at a 50 kHz sampling rate. The sampling rate in the measurements are usually set to 25 kHz. MC-Rack allows the user to select the channels for recording. MC-Rack saves files with .mcd extension containing data for all the recorded channels.

4.2.4 Isolation and mounting of retina

The isolation of the retina from the eye and the pigment epithelium abolishes regeneration of photopigment in the outer segment of the photoreceptors. The retina is thus dark adapted to preserve photopigment. To achieve this, the mouse is placed in complete dark for more than an hour before starting the experiment.

Mouse ($C57BL/6J$) is chosen from the age group 3-4 months. It is euthanized in ether in dim red light. Eyes are enucleated from the skull. The skin is stretched and pressed to push the eye out. A pair of scissors is then placed below the eye and the optic nerve is cut. The eyes are immediately dipped into constantly oxygenated Ames' Medium in a petri dish, which is transferred to the upright stage of the dissection microscope. The eyes are also dark adapted for atleast 30 min.

The eye dissection is performed under an upright microscope in dim red light. The mouse eye is $3-4$ mm in diameter and the operation is difficult with naked eye. The surgical instruments include two pairs of tweezers, a scalpel and a pair of scissors. They are cleaned with ethanol before and after the dissection. Fig. 4.3 schematically shows the retina isolation procedure.

Eye is perforated using a surgical blade and cut just behind the ora serrata into two hemispheres. Anterior half with cornea, lens and vitreous is discarded. The posterior half has the retina. It is flattened by making small cuts on the margins.

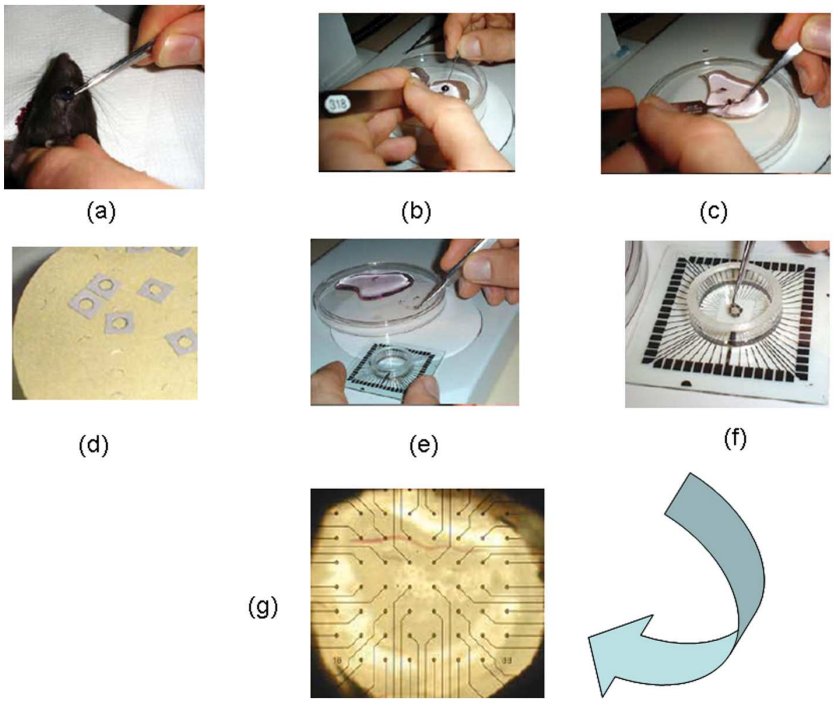

Figure 4.3: *(a-f) The steps involved in the isolation of the Retina. (g) The image of an isolated retina tissue on a TiN array taken using a stereo-microscope (magnification 30X).*

Flattened retina can be mounted onto the electrode substrate with or without the sclera.

A filter paper carrier with a punched hole is used for this purpose. The isolated retina is placed with ganglion cell side up onto a piece of nitrocellulose filter paper (40 μm, White SCWP, 13 mm, Millipore Inc.) 7mm in diameter. The filter paper is placed onto the MEA grid such that the retinal ganglion cells contact the micro-electrodes. After placement of the isolated retina onto the MEA grid, the contact pads of MEA are wiped with ethanol. The MEA is placed in its holder and the voltage amplifier is clamped onto it. The MEA recording chamber is then filled with oxygenated Ames' medium.

The Ames' Medium

Ames' Medium is a widely used medium for maintaining central nervous system tissues in vitro. It is obtained from Sigma Aldrich as a white hygroscopic powder. Around 700 ml of distilled water is bubbled with 100 % CO_2. While gently stirring the water, 1.9 g of sodium bicarbonate powder is added. The powdered Ames' medium is then added to this solution. The solution is stirred until dissolved. Additional water is then added to bring the solution to final volume. The pH can be adjusted 1 M HCl or 1 M NaOH. The medium is then equilibrated with 95% O_2 and 5% CO_2 (carbogen) and maintained at 37 ^{o}C.

4.2.5 Signal Recording

The voltage signal recording data is done using the software MC-Rack. 15 data streams (channels) are visualized on the computer screen. If on any channel, excessive noise is present, it is grounded. The whole experiment is kept in this state

for about 1-1.5 hr.

The visual stimulus is turned on and data are recorded for multiple presentations of the visual stimulus. The standard response from a healthy retina whole mount on MEA consists of slow field potentials and fast potential spikes. The data is saved for 'offline' analysis. To observe the slow field potential (electroretinogram or the ERG), standard filter settings are 0.3 Hz to 300 Hz while for spike analysis, filter is usually set to 200 Hz- 4 kHz.

4.2.6 Modification of MEA with PEDOT:PSS

After recording the data from the standard MEA, the MEA is cleaned using the procedure described above and dried in air. PEDOT:PSS dispersion (Baytron P) is filtered using a filter paper. Using a pipette, 10 μl of the filtered polymer dispersion is then spin coated in the recording area of the MEA grid. The modified MEA is put in oven at 60 ^{o}C for 20 min for the polymer film to get annealed.

4.3 Observations and Results

The recorded data from bare and PEDOT modified MEA was replayed in MC-Rack software. Following are the main features:

1. ERGs could be observed upon full field photo-stimulation with Butterworth 2nd order filter (within MC-rack) set to 0.3 Hz to 300 Hz, while the spikes were observed with the same filter set to 200 Hz- 4 kHz (Fig. 4.4).

2. PEDOT:PSS coating reduced the average base noise level of all the electrodes (Fig. 4.5).

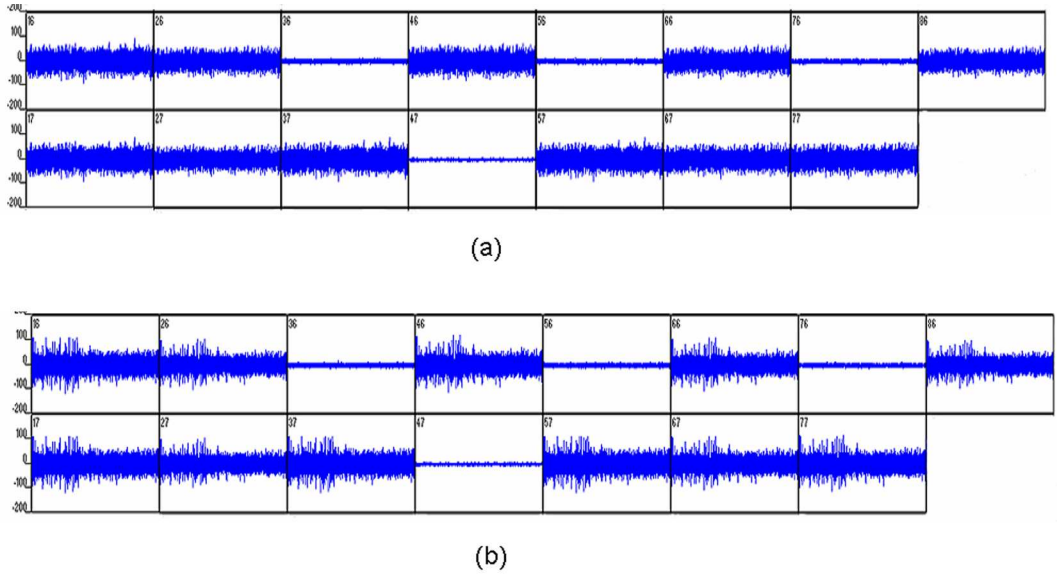

Figure 4.4: *Typical spike output from ganglion cells of a retina recorded using TiN MEA. (a) No visual stimulus. (b) Visual stimulus produces spikes output in the ganglions. The above data is recorded using 200 Hz to 4 kHz band-pass filter.*

3. The magnitude of ERGs increased by about 75% after PEDOT:PSS coating (Fig. 4.6). In fact, the light induced signals from the polymer coated electrodes had additional features.

4.4 Data and Noise Analysis

Detection of fast events like action potentials in extracellular MEA recordings is quite challenging. Existing spike detection techniques usually involve amplitude thresholds to discriminate spike events [95]. However, when signal to noise (S/N) ratio is low, the requirement of amplitude thresholds may not be sufficient.

It was observed that at times, using the offline high pass filter of the MC-Rack software, spikes could not be detected in the data obtained from the two type of MEAs. To extract information from such noisy signals recorded from MEAs, Fourier transform technique was used. The next section describes the steps

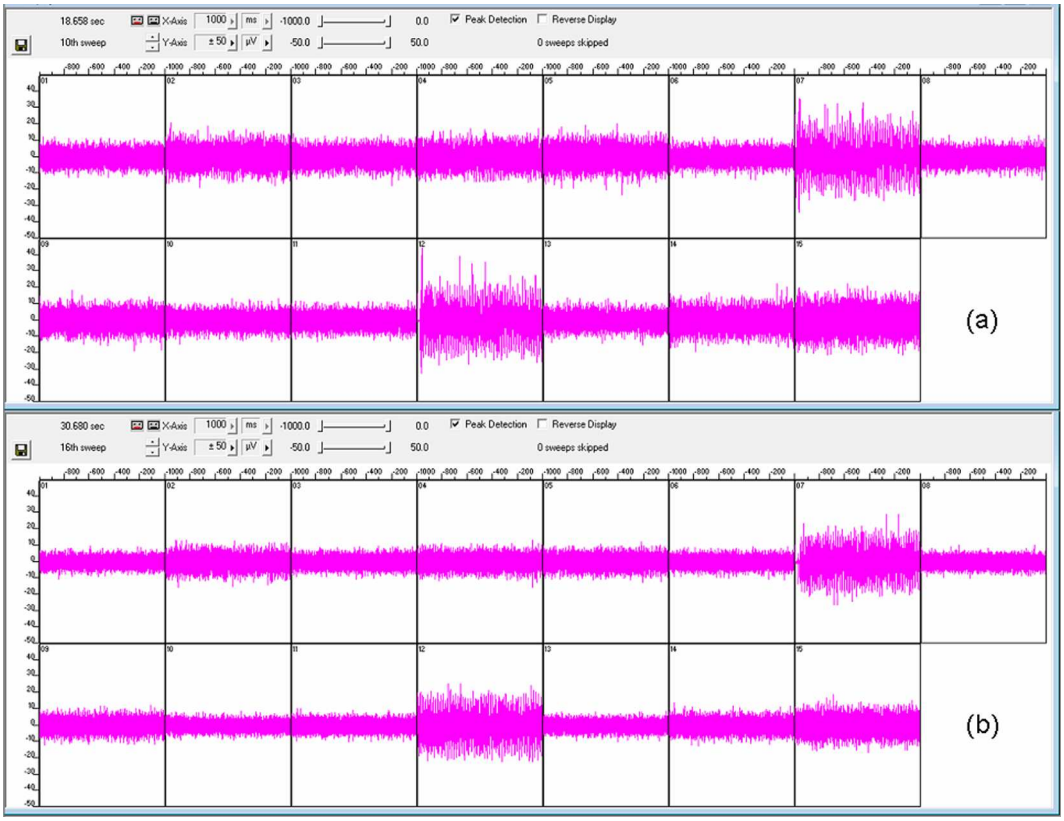

Figure 4.5: *(a) Typical noise levels on 15 channels from an ITO MEA. (b) Noise levels on all electrodes reduce after coating the electrodes with PEDOT:PSS thin film. The data shown is 100 kHz high pass filtered data.*

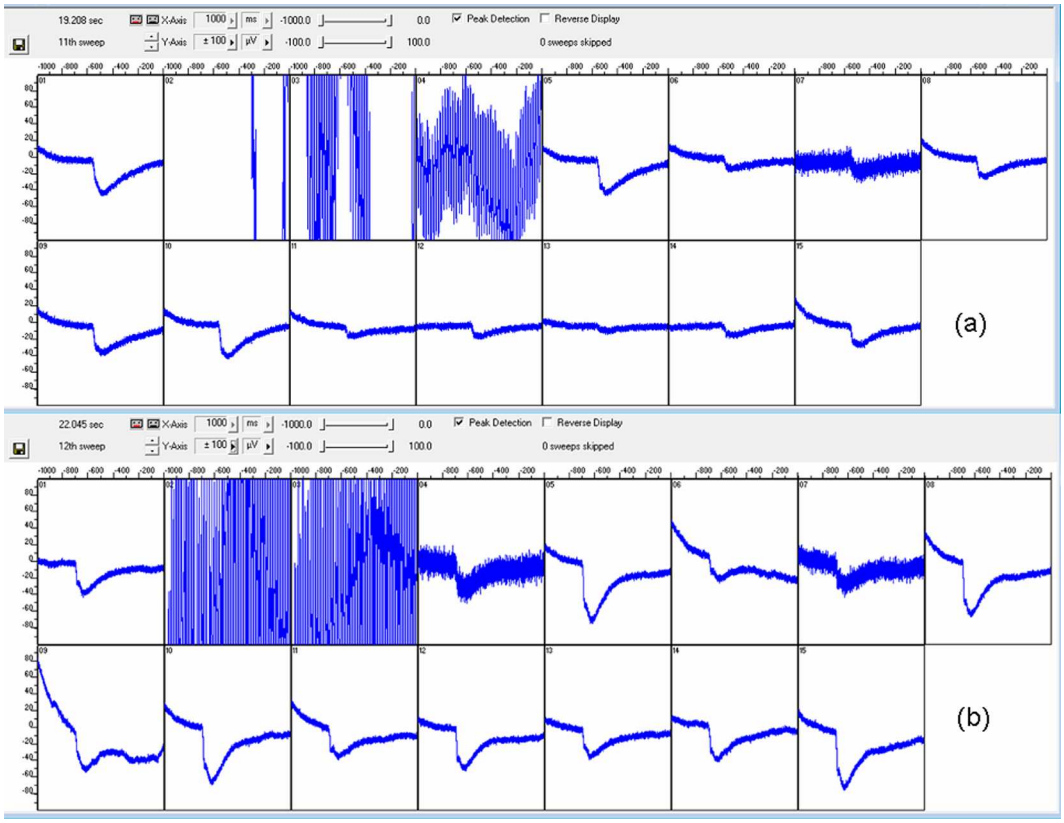

Figure 4.6: *(a) ERGs recorded from an ITO MEA (b) ERGs increase in amplitude and features when the MEA is coated with PEDOT:PSS. The data are recorded using 0.3-300 Hz band-pass filter.*

followed.

4.4.1 Methods

1. Raw data from one electrode is selected. Two windows are taken: one where light pulse was off (no stimulus) and one where it was on (stimulus). This data is sampled at 25 kHz and each window size is 1000 ms.

2. Using MC-datatool software, each of the data streams is extracted and converted from .mcd to .dat format.

3. Using Matlab, a running average of the data is done (usually 100 points). The original data is subtracted from the averaged data. This step eliminates the low frequency field potential (ERG).

4. This data set is then fed into the Matlab code written for the discrete Fourier transformation (FFT) from time domain to frequency domain (ω) as per the following expression:

$$x(\omega) = \sum_{i=0}^{n-1} x(t) \exp(-i2\pi t\frac{k}{n}) \text{ where } k = 0, 1, 2.....n-1 \tag{4.1}$$

5. N-point FFT is done (usually, N=4096). Frequency resolution is around 12 Hz.

6. The respective frequency spectra of these data sets are compared to obtain specific features.

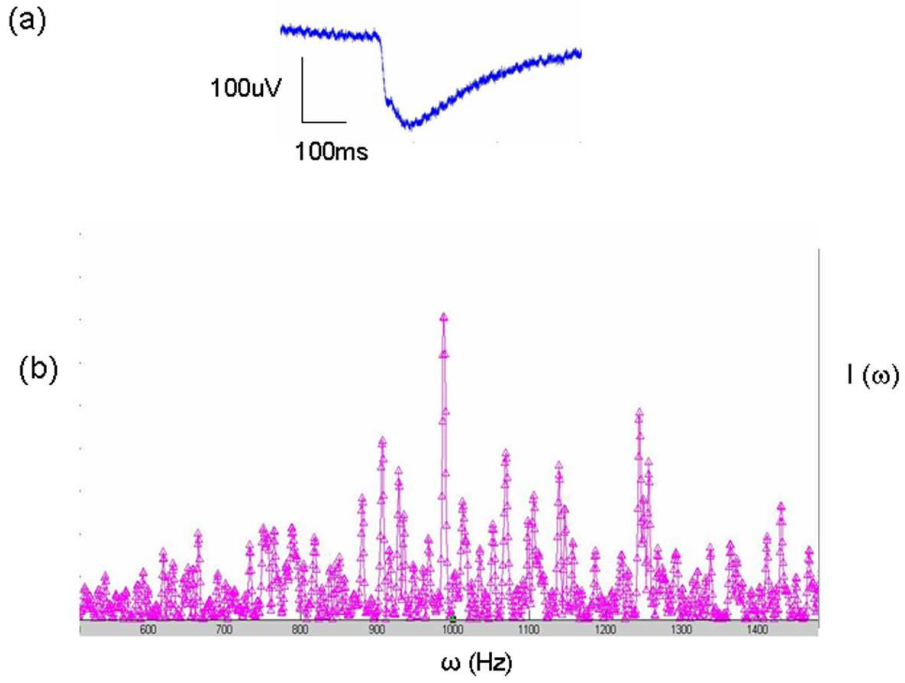

Figure 4.7: *(a) A raw data stream recorded from Hexa MEA (TiN) and (b) corresponding frequency spectrum exhibiting characteristic frequencies.*

4.4.2 Results

It was observed that the Fourier transformation of real time signals from non-stimulated ganglions was featureless with a general trend of I(ω) decreasing in with increasing ω. However, the spectrum obtained from the data collected from the stimulated ganglion cells consisted of additional features that included characteristic frequencies in the range 500 Hz-1.5 kHz (Fig. 4.7).

This signature can be interpreted to correspond to action potentials of 0.5 ms-5 ms duration.

4.5 Discussion

The MEA disk electrodes record the field changes with respect to the bath electrode. A visual stimulus on a retina whole mount produces a field gradient across the top layer (photoreceptors) and the bottom layer near the electrodes (ganglions) which appears as the ERG. It has been observed that slow components in the MEA recordings also arise due to the EPSP from bipolar to the ganglions [96]. Moreover, the output of the ganglion cells is in form of action potentials. The action potentials cause fast changes in the local field around the electrodes underneath and hence appear as spikes in the MEA recording.

Conducting polymer PEDOT:PSS intermediate layer improves the adhesion of tissue onto the standard Multi-electrode Arrays. Though both ITO and PEDOT film surfaces are flat, PEDOT has a 'softer' modulus that allows the film to get deformed when it comes in contact with a tissue. This provides a better mechanical contact between the tissue and the bottom surface. Hence, the light induced signals from the polymer coated electrodes were more appreciable in magnitude as

well as features. The signal enhancement or improved S/N ratio can arise from the enhanced surface area and close electrical contact for signal transmission.

PEDOT:PSS is a patternable electrode. It has also been shown recently that the conductivity of PEDOT:PSS films can be improved to up to 250 kS/s using specific post annealing solvent treatments [97]. This implies that PEDOT:PSS can replace the underneath metal or metal oxide electrodes in an MEA. Further, the glass chips can be replaced by patterning PEDOT:PSS electrodes on flexible substrates. This would be quite useful for in-vivo extracellular recordings.

Fourier transformation is shown to be a useful method of data mining from the MEA data when the signal to noise ratio is quite low. This method could detect additional features in a data region where no spikes were observed otherwise. This method of noise analysis has not been used previously for MEA recordings.

The power spectrum obtained from Fourier transform of the autocorrelation function taken with appropriate time lags can still provide additional information. The present efforts are directed towards verifying this analysis procedure and interpretation with enhanced signals from modified arrays. We propose that this method of noise analysis will be useful in specific issues of a problem where most of the aspects are known but only certain changes need to be investigated.

A direct analogy can also be made with the conjugated polymers used to study electrolyte interfaces the retina whole mount. Morphologically similar structures are present in both conjugated polymers and the retina that lead to their photosensitivity. Interestingly, voltage spikes observed from the conjugated polymer in

contact with a buffer solution closely resemble the signal profiles from the retina. Moreover, the polymers are compatible with the Ames' medium used as a buffer for the retina.

These features imply that conjugated polymer layers can act as the photoreceptors and transport layers in an 'Artificial Retina' based on organic materials.

References

[1] A. J. Heeger; Semiconducting and metallic polymers: The fourth generatin of polymeric materials (Noble Lecture), *Angew. Chemie. Int. Ed.*, **2001**, *40*, 2591–2611.

[2] C. K. Chiang; C. R. Fincher Jr.; Y. W. Park; A. J. Heeger; H. Shirakawa; E. J. Louis; S. C. Gau; A. G. MacDiarmid; Electrical conductivity in doped polyacetylene, *Phys. Rev. Lett.*, **1977**, *39*, 1098–1101.

[3] R. Peierls, *Qauntum Theory of Solids;* Oxford, 1995.

[4] A. J. Heeger; Nobel Lecture: Semiconducting and metallic polymers: The fourth generatin of polymeric materials, *Rev. Mod. Phys.*, **2001**, *73*, 681–700.

[5] H. Shirakawa; E. J. Louis; A. G. MacDiearmid; C. K. Chiang; A. J. Heeger; Synthesis of electrically conducting organic polymers: halogen derivatives of polyacetylene, (CH)$-x$, *J. Chem. Soc. Chem. Commun.*, **1977**, pages 578–580.

[6] C. K. Chiang; S. C. Gau; R. Fincher Jr.; Y. W. Park; A. G. MacDiarmid; A. J. Heeger; Polyacetylene, (CH)$-x$: n-type and p-type doping and compensation, *Appl. Phys. Lett.*, **1978**, *33*, 18–20.

[7] J-P. Farges, *Organic Conductors: fundamentals and application;* Marcel Dekker, 1994.

[8] P. J. Nigrey; A. G. MacDiarmid; A. J. Heeger; Electrochemistry of polyacetylene, $(CH)_x$: electrochemical doping of (CH)$-x$ films to the metallic state, *J. Chem. Soc. Chem. Commun.*, **1979**, *93*, 594–595.

[9] C. Jones; P. M. Jordan; A. G. Chaudhry; M. Akhtar; Stereospecificity of hydrogen removal from the four methylene bridges in haem biosynthesis: specific incorporation of the 11 *pro*-S hydrogen of porphobilinogen into haem, *J. Chem. Soc. Chem. Commun.*, **1979**, pages 96–97.

[10] R. D. Bach; D. H. Lucast; Stereochemistry of concerted 1,2-vinyl migration to a developing carbenium-ion centre, *J. Chem. Soc. Chem. Commun.*, **1979**, pages 593–594.

[11] M. R. Gandhi; P. Murray; G. M. Spinks; G. G. Wallace; Mechanism of electromechanical actuation in polypyrrole, *Synth. Met.*, **1995**, *73*, 247–256.

[12] S. Chao; M. S. Wrighton; Characterization of a solid-state polyaniline-based transistor: water vapor dependent characteristics of a device employing a poly(vinyl alcohol)/phosphoric acid solid-state electrolyte, *J. Am. Chem. Soc.*, **1987**, *109*, 6627–6631.

[13] D. Nilsson; T. Kugler; P. Svensson; M. Berggren; An all-organic sensortransistor based on a novel electrochemical transducer concept printed electrochemical sensors on paper, *Sens. Actuators B*, **2002**, *86*, 193–197.

[14] Z. Zhu; J. T. Mabeck; C. Zhu; N. C. Cady; C. A. Batt; G. G. Malliaras; A simple poly(3,4-ethylene dioxythiophene)/poly(styrene sulfonic acid) transistor for glucose sensing at neutral pH, *Chem. Commun.*, **2004**, pages 1556–1557.

[15] K. Krishnamoorthy; R. S. Gokhale; A. Q. Contractor; A. Kumar; Novel label-free DNA sensors based on poly(3,4-ethylenedioxythiophene, *Chem. Commun.*, **2004**, pages 820–821.

[16] X. Cui; J. F. Hetke; J. A. Wiler; D. J. Anderson; D. C. Martin; Electrochemical deposition and characterization of conducting polymer polypyrrole/PSS on multichannel neural probes, *Sens. Actuators, B*, **2001**, *93*, 8–18.

[17] J. Yang; K. Lipkin; D. C. Martin; Electrochemical fabrication of conducting polymer poly(3,4-ethylenedioxythiophene) (PEDOT) nanofibrils on microfabricated neural prosthetic devices, *J. Biomater. Sci. Polymer Edn.*, **2007**, *18*, 1075–1089.

[18] K. Hyodo; Electrochromism of conducting polymers, *Electrochim. Acta.*, **1994**, *39*, 265–272.

[19] M.-A. De Paoli; G. Casalbore-Miceli; E. M. Girotto; W. A. Gazotti; All polymeric solid state electrochromic devices, *Electrochim. Acta.*, **1999**, *44*, 2983–2991.

[20] P. Somani; A. B. Mandale; S. Radhakrishnan; Study and development of conducting polymer-based electrochromic display devices, *Acta. Mater.*, **2000**, *48*, 2859–2871.

[21] C. Arbizzani; A. Bongini; M. Mastragostino; A. Zanelli; G. Barbarella; M. Zambianchi; Polyalkylthiophenes as electrochromic materials: A comparative study of poly(3-methylthiophenes) and poly(3-hexylthiophenes), *Adv. Mater.*, **1995**, *7*, 571–574.

[22] S. A. Sapp; G. A. Sotzing; J. R. Reynolds; High contrast ratio and fast-switching dual polymer electrochromic devices, *Chem. Mater.*, **1998**, *10*, 2101–2108.

[23] Bayer AG; *European Patent*, **1988**, *03339340*.

[24] L. Groenendaal; F. Jonas; D. Freitag; H. Pielartzik; J. R. Reynolds; Poly(3,4-ethylenedioxythiophene) and its Derivatives: Past, present, and future, *Adv. Mater.*, **2000**, *12*, 481–494.

[25] F. Jonas; L. Schrader; Conductive modifications of polymers with polypyrroles and polythiophenes, *Synth. Met.*, **1991**, *41-43*, 831–836.

[26] G. Heywang; F. Jonas; Poly(alkylenedioxythiophene)s - new, very stable conducting polymers, *Adv. Mater*, **1992**, *4*, 116–118.

[27] I. Winter; C. Reese; J. Hormes; G. Heywang; F. Jonas; The thermal ageing of poly(3,4-ethylenedioxythiophene). An investigation by X-ray absorption and X-ray photoelectron spectroscopy, *Chem. Phys.*, **1995**, *194*, 207–213.

[28] M. Dietrich; J. Heinze; G. Heywang; F. Jonas; Electrochemical and spectroscopic characterization of polyalkylenedioxythiophenes, *J. Electroanal. Chem.*, **1994**, *369*, 87–92.

[29] Bayer AG; *European Patent*, **1993**, *533671*.

[30] Bayer AG; *European Patent*, **1995**, *686662*.

[31] F. Jonas; G. Heywang; Technical applications for conductive polymers, *Electrochim. Acta*, **1994**, *39*, 1345–1347.

[32] F. Jonas; J.T. Morrison; 3,4-polyethylenedioxythiophene (PEDT): Conductive coatings technical applications and properties, *Synth. Met.*, **1997**, *85*, 1397–1398.

[33] J. Ouyang; C.-W. Chu; F.-C. Chen; Q. Xu; Y. Yang; High-Conductivity Poly(3,4-Ethylenedioxythiophene):Poly(styrenesulfonate) film and its application in polymer optoelectronic devices, *Adv. Funct. Mater.*, **2005**, *15*, 203–208.

[34] M. X. Chen; Printed electrochemical devices using conducting polymers as active materials on flexible substrates, *Proc. IEEE*, **2005**, *93*, 1339–1347.

[35] Q. Peng; Z. Y. Lu; Y. Huang; M. G. Xie; D. Xiao; D. C. Zou; Novel light-emitting polymers derived from fluorene and maleimide, *J. Mater. Chem.*, **2003**, *13*, 1570–1574.

[36] D. Chirvase; Z. Chiguvare; M. Knipper; J. Parisi; V. Dyakonov; J. C. Hummelen; Temperature dependent characteristics of poly(3 hexylthiophene)-fullerene based heterojunction organic solar cells, *J. App. Phys.*, **2003**, *93*, 3376–3383.

[37] H. Rost; J. Ficker; J. S. Alonso; L. Leenders; L. McCulloch; Air-stable all-polymer field-effect transistors with organic electrodes, *Synth. Met.*, **2004**, *145*, 83–85.

[38] P. W. Anderson; Absence of diffusion in certain random lattices, *Phys. Rev.*, **1985**, *109*, 1492–1505.

[39] A. Miller and E. Abrahams; Impurity conduction at low concentrations, *Phys. Rev.*, **1960**, *120(3)*, 745–755.

[40] N. F. Mott; E. Davis, *Electronic processes in non-crystalline materials;* Clarendon Press, Oxford.

[41] R. Farchioni and G. Grosso, *Organic Electronic Materials;* Springer, 2001.

[42] I.H. Campbell; T.W. Haggler; D.L. Smith and J.P. Ferraris; Direct measurements of conjugated polymer electronic excitation energies using metal/polymer/metal structures, *Phys. Rev. Lett.*, **1996**, *76(11)*, 1900–1903.

[43] J. J. M. Halls, K. Pichler, R. H. Friend, S. C. Moratti, and A. B. Holmes; Exciton diffusion and dissociation in a poly(p-phenylenevinylene)/C[sub 60] heterojunction photovoltaic cell, *Applied Physics Letters*, **1996**, *68*(22), 3120–3122.

[44] J.J.M. Halls and R.H. Friend; The photovoltaic effect in a poly(p-phenylenevinylene)/perylene heterojunction, *Synthetic Metals*, **1997**, *85*(1-3), 1307 – 1308.

[45] V. Choong, Y. Park, Y. Gao, T. Wehrmeister, K. Mullen, B. R. Hsieh, and C. W. Tang; Dramatic photoluminescence quenching of phenylene vinylene oligomer thin films upon submonolayer Ca deposition, *Applied Physics Letters*, **1996**, *69*(10), 1492–1494.

[46] C. W. Tang; Two-layer organic photovoltaic cell, *Applied Physics Letters*, **1986**, *48*(2), 183–185.

[47] G. Yu, J. Gao, J. C. Hummelen, F. Wudl, and A. J. Heeger; Polymer Photovoltaic Cells: Enhanced Efficiencies via a Network of Internal Donor-Acceptor Heterojunctions, *Science*, **1995**, *270*(5243), 1789–1791.

[48] J. J. M. Halls; C.A. Walsh; E.A. Greenham; N.C. Marseglia; R.H. Friend; S.C. Moratti; A.B. Holmes; Efficient photodiodes from interpenetrating polymer networks, *Nature*, **1995**, *376*, 498.

[49] C. J. Brabec; N. S. Sariciftci; J. C. Hummelen; Plastic Solar Cells, *Advanced Functional Materials*, **2001**, *11*(1), 15–26.

[50] N. S. Sariciftci; L. Smilowitz; A. J. Heeger; and F. Wudl; Photoinduced Electron Transfer from a Conducting Polymer to Buckminsterfullerene, *Science*, **1992**, *258*, 1474.

[51] Tracey M. Clarke and James R. Durrant; Charge Photogeneration in Organic Solar Cells, *Chem. Rev.*, **2010**, *xxxx*(xxx), 000.

[52] F. Padinger; R.S. Rittberger; N. S. Sariciftci; Plastic Solar Cells, *Advanced Functional Materials*, **2003**, *13*, 85.

[53] Youngkyoo Kim, Stelios A. Choulis, Jenny Nelson, Donal D. C. Bradley, Steffan Cook, and James R. Durrant; Device annealing effect in organic solar cells with blends of regioregular poly(3-hexylthiophene) and soluble fullerene, *Applied Physics Letters*, **2005**, *86*(6), 063502.

[54] C. J. Brabec; Organic photovoltaics, *Sol. Energy Mater. Sol. Cells*, **2004**, *83*, 273.

[55] By Paul W. M. Blom; Valentin D. Mihailetchi; L. Jan Anton Koster; Denis E. Markov; Device Physics of Polymer:Fullerene Bulk Heterojunction Solar Cells, *Adv. Mat.*, **2007**, *19*, 1551–1566.

[56] Matthias Muntwiler; Qingxin Yang; William A. Tisdale; and X.Y. Zhu; Coulomb Barrier for Charge Separation at an Organic Semiconductor Interface, *Phy. Rev. Lett.*, **2008**, *101*, 196403.

[57] H. Gerischer; Impact of semiconductors on the concepts of electrochemistry, *Electrochim. Acta*, **1990**, *35*, 1677–1699.

[58] R. Memming and G. Schwandt; Potential distribution and formation of surface states at the siliconelectrolyte interface, *Surf. Sci.*, **1996**, *4*, 109.

[59] M. X. Tan; C. N. Kenyon and N. S. Lewis; Experimental measurement of quasi-Fermi levels at an illuminated semiconductor/liquild contact, *J. Phys. Chem.*, **1994**, *98*, 4959.

[60] H. Gerischer and M. Lubke; On the etching of silicon by oxidants in ammonium fluoride, *J. Electroanal.Chem.*, **1995**, *135*, 2782.

[61] P. C. Searson and X. G. Zhang; The anodic dissolution of silicon in HF solutions, *J. Electrochem. Soc.*, **1990**, *137*, 2539.

[62] I.K. Kovacs and G. Horvai; Possibilities of chemical sensing at the semiconductor/electrolyte interface, *Sensors and Actuators B*, **1994**, *18*, 315–320.

[63] Micha Tomkiewics; Impedance specetroscopy of rectifying semiconductor-electrolyte interfaces, *Electrochim. Acta*, **1990**, *35*, 1631–1635.

[64] V.M.Arutyunyan; Physical Properties of the semiconductor-electrolyte interfaces, *Sov. Phys. Usp*, **1989**, *32(6)*, 521.

[65] P. M. M. Bressers; J. W. J. Knapen; and E. A. Meulenkamp; Visible light emission from a porous silicon/solution diode, *J. Electroanal.Chem.*, **1992**, *61*, 108.

[66] M. R. Antognazza, D. Ghezzi, D. Musitelli, M. Garbugli, and G. Lanzani; A hybrid solid-liquid polymer photodiode for the bioenvironment, *Applied Physics Letters*, **2009**, *94*(24), 243501.

[67] Wenfang Zhang; P. Schmidt-Zhang; G. Kossmehl; W. Plieth; Photocurrent and differential capacity measurements at polybithienyl and poly(3-butylthiophene), *J. Solid State Electrochem.*, **1999**, *3*, 135–140.

[68] Peiqing Yu; Denis Mencaraglia; Arouna Darga; Anne Migan; Roshanak Rabdbeh; Bernard Ratier; Andr Moliton; Investigation of electric charge transport in conjugated polymer P3HT: PCBM solar cell with temperature dependent current and capacitance measurements, *Physica Status solidi (c)*, **2010**, *7(3)*, 1000–1004.

[69] He Yan1; Zhihua Chen1; Yan Zheng1; Christopher Newman1; Jordan R. Quinn1; Florian Dtz2; Marcel Kastler3 and Antonio Facchetti; A high-mobility electron-transporting polymer for printed transistors, *Nature*, **2009**, *457*, 679–686.

[70] Norio Sato, *Electrochemistry at metal and semiconductor electrodes;* Elsevier, 2003.

[71] Allen J. Bard and Larry R. Faulkner, *Electrochemical Methods (Fundamentals and applications);* Wiley-India, 2006.

[72] Y.B.Wang; R.K. Yuan and M. Willander; Capacitance of semiconductor-electrolyte junction and its frequency dependence, *Applied Physics A*, **1996**, *63*, 481–486.

[73] Andreas Stadler and Markus Burghart; Organic-MISTFT Capacitance Measurements, *IEEE Transactions on Dielectrics and Electrical Insulation*, **2006**, *13(4)*, 850–854.

[74] Mikhail I. Rabinovich; Dynamical Principles in Neuroscience, *Rev. Mod. Phys.*, **2006**, *78*.

[75] Eric. R. Kandel; James Schwartz ; Thomas Jessell, *Principles of Neural Science;* Mc-Graw Hill, 2000.

[76] K.S. Cole and H.J. Curtis; Electric Impedance of the Squid Giant Axon during Activity, *J. Gen. Physiol.*, **1939**, *22*, 649–670.

[77] A.F. Hodgkin and A.F. Huxley; Measurement of current-voltage relations in the membrane of the giant axon of Loligo, *J. Physiol.*, **1952**, *116*, 424–448.

[78] A.F. Hodgkin and A.F. Huxley; Currents carried by sodium and potassium ions through the membrane of the giant axon of Loligo, *J. Physiol.*, **1952**, *116*, 449–472.

[79] A.F. Hodgkin and A.F. Huxley; The components of membrane conductance in the giant axon of Loligo, *J. Physiol.*, **1952**, *116*, 473–496.

[80] A.F. Hodgkin and A.F. Huxley; A quantitative description of membrane current and its application to conduction and excitation in nerve, *J. Physiol.*, **1952**, *117*, 500544.

[81] E. Neher and B. Sakmann; Single-channel currents recorded from membrane of denervated frog muscle fibres, *Nature*, **1976**, *260*, 799–802.

[82] Areles Molleman, *Patch Clamping: An Introductory Guide To Patch Clamp Electrophysiology;* John Wiley and Sons Ltd., 2003.

[83] A. Stett; U. Egert; E. Guenther; F. Hofmann; T. Meyer; W. Nisch and H. Haemmerle; Biological application of microelectrode arrays in drug discovery and basic research, *Anal Bioanal Chem*, **2003**, *377*, 486–495.

[84] C.A. Thomas; P.A. Springer; G.E. Loeb; Y. Berwald-Netter; L.M. Okun; A miniature microelectrode array to monitor the bioelectric activity of cultured cells, *Exp. Cell. Res.*, **1972**, *74*, 61–66.

[85] H. Kolb; How the Retina Works, *Amer. Sci.*, **2003**, *91*, 28–35.

[86] C.D. James; R. Davis M. Mayer; A. Turner; G. Withers; L. Kam; G. Banker; H. Craighead; M. Issacson; J. Turner and W. Shain; Aligned microcontact printing of micrometer scale ploy-l-lysine structures for controlled growth of cultured neurons on planer microelectrode arrays, *IEEE Transactions on Biomedical Engineering*, **2000**, *47(1)*, 17.

[87] Y. Fang; A.B. Greytak; G. Zheng F. Patolsky; B.P. Timko; G. Yu and C.M. Lieber; Detection, Stimulation, and Inhibition of Neuronal Signals with High-Density Nanowire Transistor Arrays, *Science*, **2006**, *313*, 1100–1104.

[88] V. Lovat; D. Pantarotto; L. Lagostena; B. Cacciari; M. Grandolfo; M. Righi; G. Spalluto; M. Prato; L. Ballerini; Carbon nanotube substrates boost neuronal electrical signaling, *Nano Lett.*, **2005**, *5(6)*, 1107–1110.

[89] Magnus Berggren and Agneta Richter-Dahlfors; Organic Bioelectronics, *Adv. Mater.*, **2007**, *19*, 32013213.

[90] Sarah M. Richardson-Burns; Jeffery L. Hendricks; Brian Foster; Laura K. Povlich; Dong-Hwan Kim and D.C. Martin; Polymerization of conducting polymer PEDOT around living neural cells, *Biomaterials*, **2007**, *28*, 1539–1552.

[91] J. Yang; K Lipkin and D.C. Martin; Electrochemical fabrication of conducting polymer PEDOT nanofibrils on microfabricated neural prosthetic devices, *J. biomater. Sci. Polymer Edn.*, **2007**, *18*, 1075–1089.

[92] M. R. Abidian and David C. Martin; Experimental and theoretical characterization of implantable neural microelectrodes modified with conducting polymer nanotubes, *Biomaterials*, **2008**, *29(9)*, 1273–1283.

[93] M. R. Abidian; J. M. Corey; D. R. Kipke and David C. Martin; Conducting polymer nanotubes improve electrical properties, mechanical adhesion, neural attachment and neural outgrowth of neural electrodes, *Small*, **2010**, *6(3)*, 431–429.

[94] M. R. Abidian; Kip. A. Ludwig; T. C. Marzullo; D. C. Martin and D. R. Kipke; Interfacing conducting polymer nanotubes with the central nervous system: Chronic Neural Recording using PEDOT Nanotubes, *Adv. Mater.*, **2009**, *21*, 3764–3770.

[95] Kim K.H. and Kim S.J.; Neural spike sorting under nearly 0-dB signal-to-noise ratio using nonlinear energy operator and artificial neural-network classifier, *IEEE Trans. Biomed. Eng.*, **2000**, *47(10)*, 1406–1411.

[96] J.S. Ye and Y.S. Goo; The slow wave component of retinal activity in rd-rd mice recorded with a multi-electrode array, *Physiology Measurements*, **2007**, *28*, 1079–1088.

[97] Joung Eun Yooa; Kwang Seok Leeb; Andres Garciac; Jacob Tarvera; Enrique D. Gomeza; Kimberly Baldwina; Yangming Sunb; Hong Mengd; Thuc-Quyen Nguyenc and Yueh-Lin Looa; Directly patternable, highly conducting

polymers for broad applications in organic electronics, *PNAS*, **2010**, *107(13)*, 5712–5717.